Title

Evolution of the ribbon-like organization of the Golgi apparatus in animal cells.

Authors

Giovanna Benvenuto[1§], Serena Leone[1§], Emanuele Astoricchio[1], Sophia Bormke[2], Sanja Jasek[3], Enrico D'Aniello[1], Maike Kittelmann[4], Kent McDonald[5], Volker Hartenstein[6], Valentina Baena[7], Héctor Escrivà[8], Stephanie Bertrand[8], Bernd Schierwater[9], Pawel Burkhardt[10], Iñaki Ruiz-Trillo[11], Gáspár Jékely[3], Jack Ullrich-Lüter[2], Carsten Lüter[2], Salvatore D'Aniello[1], Maria Ina Arnone[1], Francesco Ferraro[1,12,] *

Authors affiliations

[1]Department of Biology and Evolution of Marine Organisms, Stazione Zoologica Anton Dohrn (SZN), Naples, Italy; [2]Museum für Naturkunde, Berlin, Germany; [3]Living Systems Institute, University of Exeter, UK; [4]Department of Biological and Medical Sciences, Oxford Brookes University, Oxford, UK; [5]Electron Microscope Lab, University of California Berkeley, Berkeley, CA, U.S.A; [6]Department of Molecular, Cell and Developmental Biology, University of California Los Angeles (UCLA), Los Angeles, CA, U.S.A.; [7]Department of Cell Biology, UConn Health, Farmington, CT, U.S.A.; [8]Sorbonne Université, CNRS, Biologie Intégrative des Organismes Marins, BIOM, F-66650, Banyuls-sur-Mer, France; [9]Institute of Ecology and Evolution, Hannover University of Veterinary Medicine Foundation, Hannover, Germany; [10]Michael Sars Centre, University of Bergen, Bergen, Norway;[11]Institut de Biologia Evolutiva (CSIC-Universitat Pompeu Fabra), Barcelona, Spain.

[§] These authors contributed equally

[12] Lead contact

* Correspondence: francesco.ferraro@szn.it

Keywords

Golgi apparatus; Golgi structure; Golgi ribbon; organelle; evolution; metazoans; GRASP, Golgin-45; AlphaFold2

Summary

The structural and functional unit of the Golgi apparatus is the stack, formed by piled membranous cisternae[1,2]. Among eukaryotes the number of stacks ranges from one to several copies per cell[3]. When present in multiple copies, the Golgi is observed in two arrangements: stacks either remain separated or link into a centralized structure referred to as the “ribbon”, after its description by Camillo Golgi[4]. This Golgi architecture is considered to be restricted to vertebrate cells and its biological functions remain unclear[3,5-9].

Here we show that the ribbon-like Golgi organization is instead present in the cells of several animals belonging to the cnidarian and bilaterian clades, implying its appearance in their common ancestor. We hypothesize a possible scenario driving this structural innovation. The Golgi Reassembly and Stacking Proteins, GRASPs, are central to the formation of the mammalian Golgi ribbon by mediating stack tethering[10-15]. To link the stacks, GRASPs must be correctly oriented on Golgi membranes through dual anchoring including myristoylation and interaction with a protein partner of the Golgin class[16,17]. We propose that the evolution of binding of Golgin-45 to GRASP led to Golgi stack tethering and the appearance of the ribbon-like organization. This hypothesis is supported by AlphaFold2 modelling of Golgin-45/GRASP complexes of animals and their closest unicellular relatives. Early evolution and broad conservation of the ribbon-like Golgi architecture imply its functional importance in animal cellular physiology. We anticipate that our findings will stimulate a wave of new studies on the so far elusive biological roles of this Golgi arrangement.

Results and Discussion

Deuterostome animals assemble Golgi ribbons. According to the current consensus, only vertebrate cells form a centralized Golgi structure with multiple stacks aligned and linked to each other. This Golgi organization is known as the ribbon and its functions remain unclear to this date[3,5,6,9,18]. We were therefore intrigued by morphological data suggestive of Golgi centralization in the embryos of two sea urchin species, *Strongylocentrotus purpuratus* and *Lytechinus variegatus*[19,20], and set out to analyze Golgi dynamics in a third one, *Paracentrotus lividus*. Time-course analysis of a fluorescent Golgi reporter showed that early in development, throughout the cleavage stage, the Golgi is present as separate elements which then cluster into centralized structures before hatching of the blastula (Figure 1A, S1A, S1B). Golgi clustering is rapid: within one hour, Golgi elements increase 10-fold in size while their number decreases 3-fold (Figure 1B, 1C and Movie S1). Afterwards, centralized Golgi complexes are observed in all cells of the embryo and at all developmental stages up to the planktonic pluteus larva (Figure 1A and S1C). Confocal imaging at higher magnification of post-clustering stages showed a morphology strongly reminiscent of the Golgi ribbon as observed in mammalian cells (Figure S1D). In mammalian cells, the Golgi ribbon can be visualized by electron microscopy[18]. We therefore analyzed sea urchin Golgi morphology at the ultrastructural level. As Golgi stack dimers have been observed in *Drosophila melanogaster* cells[21], which notoriously display dispersed Golgi elements[22], and even in mammalian cells after ribbon unlinking by microtubule depolymerization[23], we defined Golgi centralization as “ribbon-like” only when three or more closely apposed stacks were observed in electron micrographs (Figure S1E). In sea urchin, at the ultrastructural level, the arrangement of Golgi elements recapitulated confocal microscopy observations. Separated stacks cluster and finally establish connections with each other during early development, confirming that sea urchins centralize their Golgi apparatus into a ribbon-like architecture (Figure 1D). Centralized Golgi complexes were previously observed in the early *Strongylocentrotus purpuratus* embryo[19]. Indeed, we also observed ribbon-like Golgis in the pluteus of this sea urchin species (Figure S1F). Like the ribbon of mammalian cells, sea urchin’s centralized Golgi undergoes disassembly/reassembly cycles during mitosis (Figure S1G) and its maintenance requires an intact microtubule network (Figure S1H-S1I)[2,5,24-26]. All these characteristics strongly indicate that the centralized Golgi complexes of sea urchin cells are indeed ribbons. Sea urchins as echinoderm representatives branch off from the deuterostome lineage at a basal position and form part of the sister group to all remaining chordates including vertebrates. Therefore, the mechanisms mediating Golgi centralization are likely to be conserved across the deuterostome clade. Indeed, we observed Golgi stack clustering and ribbon-like formation during development in cells of two non-vertebrate chordates, the sea squirt *Ciona robusta* (tunicate) and the lancelet *Branchiostoma*

lanceolatum (cephalochordate) (Figure 1E and 1F). As Golgi centralization also occurs in mammalian early embryos[27], our observations not only show that it is a conserved feature across deuterostomes, but also suggest that it might play a role during the initial stages of their development. Our findings also raise the intriguing possibility that Golgi centralization may have evolved before the split between deuterostomes and other animal groups. If this were the case, then centralization of Golgi stacks should be also observed in non-deuterostomes.

Golgi architecture in holozoans. By examining published and newly generated data, we surveyed Golgi ultrastructure in representatives of several animal taxa and closely related unicellular eukaryotes, which, together, comprise the eukaryotic holozoan clade. Ribbon-like presence was assessed by adopting the criterion used for sea urchin and other deuterostomes (Figure S1E). In mammals, ribbon architecture, though widespread, is not ubiquitous. Differentiated tissues such as muscles, acid-secreting gastric cells, and spinal ganglion neurons, for instance, display Golgi complexes made by separated stacks[28-30]. For this reason, wherever possible, several cell types of the organisms under consideration were inspected. We first set out by looking at bilaterians other than deuterostomes. In the cells of the marine worm *Symsagittifera roscoffensis* (xenacoelomorph), separated stacks were observed (not shown). Interestingly, some of its secretory cells displayed closely apposed, though clearly distinct, Golgi stacks: an intermediate organization between separated Golgi elements and a ribbon-like organization (Figure 2A and S2A). Ribbon-like Golgis were found in epidermal cells of the three-lobed larva of the brachiopod *Calloria inconspicua* and in several cell types of the marine annelid *Platynereis dumerilii* (Figures 2B, 2C, S2B and Movie S2). As Ramón y Cajal described ribbon-like Golgis in neurons and epithelial cells of the common earthworm[31], we conclude that this Golgi organization is common among annelids. In mollusks, a centralized Golgi that fragments at mitosis was observed in spermatocytes of the snail *Paludina vivipara* more than a century ago[32], while other reports show ribbon-like Golgi complexes in other species (e.g., *Helix pomatia*[33] and *Helix aspersa*[34]). Cells of the fruit fly *Drosophila melanogaster*, an arthropod, and of the roundworm *Caenorhabditis elegans*, a nematode, two model organisms widely used in genetics and cell biology, display Golgi complexes consisting of several, separated stacks[21,22,35,36]. To test whether Golgi stack decentralization is an arthropod feature, as opposed to *Drosophila*/insect-specific, we analyzed the ultrastructure of the crustacean *Parhyale hawaiensis*, observing separated stacks in neurons (Figure 2D) and in all other inspected cell types (not shown). It is therefore likely that a decentralized Golgi is the typical configuration in arthropods, not just of *Drosophila* and other insects (e.g., bees, aphids and mosquitos[37-39]). We then analyzed cnidarians: in the hydrozoan *Clytia hemisphaerica*, the

secretory gland cells of the gastroderm, but not other cell types, display stacks linked into a ribbon-like structure (Figure 2E), which is also observed in phagocytic cells of another cnidarian, the actinia *Phelliactis robusta*[40]. In the ctenophore *Mnemiopsis leidyi*, epithelial and comb cells (Figure 2F and S2E), nerve net neurons, mesogleal neurons, and sensory cells[41,42] all display separated stacks. Among other animals, we found a single Golgi stack in all cells of two placozoan species: *Trichoplax adhaerens* (Figure 2G, S2C and S2D) and *Hoilungia hongkongensis*[43]. Like placozoans, the sea sponge *Oscarella carmela* (Figure 2H and reference[44]) and other species (genera *Chondrosia*, *Crambe* and *Petrosia*; not shown) have a single Golgi stack per cell.

In choanoflagellates and filastereans, which are unicellular holozoans, the Golgi is also present as a single stack per cell (Figure 2I and references[44,45]). In summary, despite a relatively small sampling (Figure S2F), ribbon-like Golgi complexes are easily observed in cells of cnidarians and bilaterians, and not found outside these animal taxa. The presence of multiple stacks per cell is a precondition for their clustering and ribbon formation, but it is not sufficient. In fact, while usually displaying a single Golgi stack per cell (Figure 2H, and reference[44]), in rare instances cells with multiple but separated stacks are observed in sponges, as is the case in the gemmule's spongocytes of the freshwater species *Ephydatia fluviatilis*[46]. It should be noted that the thin sectioning of electron micrographs does not allow to assess whether all the Golgi stacks in a cell are linked into a single ribbon-like organization or form multiple "mini-ribbons". Nonetheless, in those cases where we identified a ribbon-like organization we can state that the process of stack centralization is clearly observed.

In conclusion, the most parsimonious explanation accounting for our results and the literature data is that the ribbon-like Golgi likely evolved in the common ancestor of cnidarians and bilaterians, and was secondarily lost in xenacoelomorphs, arthropods, and nematodes (Figure 2J).

Putative molecular mediators of ribbon-like Golgi emergence. Next, we asked which molecular innovations might have driven the emergence of the ribbon-like Golgi organization. If, as our survey suggests, this was a single evolutionary event, conservation of the molecular mechanisms of its formation would be expected. Among the several factors involved in the formation of the mammalian Golgi ribbon[26,47-56], the molecular tethers GRASP (Golgi Reassembly and Stacking Protein) and the coiled-coil proteins collectively known as Golgins play a central role[8,10-12,15,16,56-60]. GRASPs comprise a highly conserved GRASP region, made of two atypical PDZ domains in tandem, and an evolutionarily more variable C-terminal unstructured region (Figure S3A and S3B). While GRASPs are encoded by a single gene in most eukaryotes, a duplication gave rise to two paralogs in jawed vertebrates

(Figure S3C and Data S1A). Involved in several cellular processes[61-64], GRASPs are capable of self-interaction and while they were initially considered to promote cisternal adhesion within the stack[58,65,66], recent work unequivocally showed that they mediate Golgi stack tethering and ribbon formation but not cisternal stacking[14,15,67]. The two mammalian paralogs, GRASP55 and GRASP65, are recruited to Golgi membranes by myristoylation of the glycine in position 2[65,68], conserved across holozoans (Data S1A), and by interaction with Golgin-45 and GM130, respectively (Figure 3A)[57,69]. Such dual-anchoring is required for ribbon formation as it spatially orients GRASPs and allows their homo-dimerization/oligomerization in *trans*, thus tethering membranes of distinct Golgi stacks and promoting ribbon formation[12,16,17]. Golgins (Figure 3A) mediate vesicular traffic specificity[70-72] and their knockdown results in secretory defects and ribbon unlinking into constituent stacks[8,73]. The Golgin-45 gene is an innovation of holozoans[74]. In mammals, the Golgin-45 protein interacts with the GRASP paralog GRASP55[57] (Figure 3A); and in cultured cells, either Golgin-45 knockdown or long-term degron-induced ablation of GRASP55, but not of GRASP65, result in Golgi ribbon unlinking[15,57]. As GRASP55 is more similar to the single GRASP proteins present in non-vertebrate bilaterians and cnidarians (Figure S3C), it is plausible that evolution of GRASP binding by Golgin-45 may have led to GRASP-mediated stack tethering (i.e., centralization) and ribbon-like Golgi evolution (Figure 3B). We searched and identified holozoan Golgin-45 homologs, confirming previous findings that this protein evolved in the common ancestor of holozoans[74] and then was lost in choanoflagellates (Data S1B). Interestingly, among metazoans, it was also lost in most xenacoelomorphs (Data S1B), which do not display ribbon-like Golgi (Figures 2A and S2A).

The crystal structure of the complex between the C-terminus of mouse Golgin-45 and the GRASP domain of the conspecific GRASP55 has been solved[75], highlighting the existence of three main interaction sites between the two proteins: i) a PDZ-binding motif spanning the four C-terminal amino acids of Golgin-45; ii) an atypical Zinc finger composed by two cysteines of Golgin-45 and a cysteine and a histidine in the GRASP domain; iii) the insertion of nine residues of Golgin-45 into the hydrophobic groove between the two PDZ domains of GRASP55 (Figure S3D)[75]. Binding experiments showed that the PDZ-binding motif and the cysteine pair are necessary for Golgin-45/GRASP complex formation, whereas the contribution of the groove-interacting residues remains unclear[75] (see the section *"Role of groove residues in Golgin-45/GRASP interaction"* of the Supplemental Results and Discussion). We aligned the C-terminal sequences of holozoan Golgin-45 proteins to assess conservation of the amino acids involved in GRASP interaction (Figure S3E). The PDZ binding motif and the cysteine pair are highly conserved, with the notable exception of *Drosophila melanogaster* and *Parhyale hawaiensis*, whose cells lack ribbon-like Golgi organization (Figure S3E, refs.[21,22] and Figure 2D), whereas the Golgin-45 residues

corresponding to those that interact with the GRASP groove are more variable across holozoans (Figure S3E).

As the AlphaFold2[76,77] model of the mouse Golgin-45/GRASP complex displayed high confidence and stability (refer to the section *"Interpretation and predictive power of AlphaFold2 models"* of the Supplemental Results and Discussion) and was very similar to the crystal structure (Figure 3C), we reasoned that Golgin-45/GRASP interactions may be predicted[78,79] by modelling complexes of conspecific protein pairs. We considered binding to occur when GRASP interaction with the PDZ-binding motif and formation of the Zinc finger could be detected in the modelled complex. In bilaterians and cnidarians, all models predicted binding, except for arthropods (*Drosophila melanogaster* and *Parhyale hawaiensis*), nematodes (*Caenorhabditis elegans*) and the only xenacoelomorph species with a Golgin-45 gene, *Hofstenia miamia* (Figures 3D and S4A). Golgin-45 was not predicted to bind its conspecific GRASP in ctenophores, porifera and unicellular filastereans (Figure 3D). The reliability of AlphaFold2 predictions was further corroborated by modeling the complexes of various point mutants of the mouse Golgin-45 PDZ-binding motif, cysteine pair, and groove interacting residues that had been experimentally tested in *in vitro* GRASP binding assays[75]. The models obtained were consistent with the experimental data by those authors[75] (Figure S4B; see also the section *"Role of groove residues in Golgin-45/GRASP interaction"* of the Supplemental Results and Discussion). Based on structure modelling and experimental evidence[75], we therefore deduce that a stable Golgin-45/GRASP interaction appeared in the common ancestor of cnidarians and bilaterians but was impaired by subsequent amino acid mutations in arthropod, nematode, and the only xenacoelomorph proteins (Figures 3E and S4A). In conclusion, AlphaFold2 models lend support to our hypothesis that the evolution of GRASP binding by Golgin-45 may have driven the appearance of stack tethering and the emergence of the ribbon-like Golgi organization.

Conclusions

The ribbon organization of the Golgi apparatus was previously considered to be unique to vertebrates. The lack of a centralized Golgi in the cells of *D. melanogaster* and *C. elegans*, two invertebrates widely used in cell biology, may have contributed to cement this view. Nonetheless, works dating to the early 1900's already showed the presence of ribbon-like Golgi complexes in non-vertebrates[31,32], and further evidence from electron microscopy analyses of various animal cells accumulated later[33,34,40,80]. Here, we built on this body of literature by sampling species representative of diverse metazoan taxa and show that ribbon-like centralization of Golgi stacks is likely to be a newly evolved character of the ancestor of cnidarians and bilaterians. The frequency with which ribbon-like Golgi complexes are found, both by our morphological analyses and in the literature, supports the

generalizations we made on its evolutionary emergence and secondary loss at the level of phyla and superphyla (Figure 2J). Based on experimental evidence from studies in mammalian cells, we also propose a plausible and testable molecular mechanism of evolution of the ribbon-like Golgi organization. GRASP "resurrection" experiments show that its self-interacting capability is ancestral[81]. Bootstrapping on this function, and in the context of cells with multiple stacks, evolution of GRASP binding activity by Golgin-45 may have driven ribbon-like emergence. Our hypothesis invokes a central role for Golgin-45/GRASP interaction in the evolution and conservation of the mechanism of formation of Golgi ribbons. Whether the Golgin-45-dependent spatial orientation of GRASP on Golgi membranes is only conducive to stack tethering or also to membrane continuity between cisternae of juxtaposed stacks, as observed in mammalian cells[18,82,83], remains to be experimentally tested. GRASP55 is necessary for ribbon formation in mammals and interacts with tens of proteins[15,84]. If such interactions are evolutionarily conserved, GRASP oligomerization could provide a molecular scaffold that directly mediates Golgi stack tethering and, indirectly, coordinates the activity of several factors in the assembly and maintenance of the Golgi ribbon.

In eukaryotes, complex multicellularity evolved several times[85], but non-animal multicellular organisms, such as plants and fungi, display multiple separated Golgi stacks[86-88]. Golgi centralization may thus indicate an evolutionary trajectory with functional requirements specific to cnidarians/bilaterians and divergent from those of other animals and multicellular organisms. The question thus arises as to which functions did the ribbon-like Golgi organization evolve to carry out. As the biological roles of the ribbon remain unclear, we can only speculate. In deuterostomes, Golgi centralization occurs in early embryogenesis (this report and reference[27]). This may indicate that the primordial function of the ribbon-like architecture could have been in development, explaining why some differentiated mammalian tissues can forgo Golgi ribbons[28-30]. In this hypothetical scenario, the developmental processes of xenacoelomorphs, arthropods and nematodes must have adapted to dispense with Golgi centralization altogether.

In conclusion, the wide occurrence of the ribbon-like Golgi organization among animals with well-differentiated cell types is strongly indicative of its functional importance. We expect that comparative functional studies in several experimental organisms, which became available in recent years, will prove successful in unravelling which functions the Golgi ribbon plays in animal cell physiology.

Acknowledgements

We thank Laura Núñez Pons, Filomena Ristoratore, and Periklis Paganos (Stazione Zoologica Anton Dohrn, SZN, Italy) for providing electron micrographs of sea sponges, of the

sea urchin *Strongylocentrotus purpuratus* and helping with the anatomy of the *Ciona intestinalis* larva; Evelyn Houliston (Villefranche-sur-mer, France) and Mark Terasaki (UConn Health, USA) for providing the *Clytia hemisphaerica* electron micrograph; Elisabeth Knust and Michaela Yuan (Max-Planck-Institute of Molecular Cell Biology and Genetics, Dresden, Germany) and Xavier Bailly (Centre National de la Recherche Scientifique & Université Pierre et Marie Curie, CNRS-PMC, Roscoff, France) for their help with *S. roscoffensis* samples; Pedro Martinez Serra (Universitat de Barcelona, Spain) for his valuable suggestions; Martin Lowe (University of Manchester, UK) and Evelyn Houliston (Villefranche-sur-mer, France) for their comments on the manuscript. Francesco Ferraro is supported by SZN intramural funding. Emanuele Astoricchio is supported by a PhD fellowship funded by the Stazione Zoologica Anton Dohrn (Open University – Stazione Zoologica Anton Dohrn PhD Program). With the aim of expanding our survey, we would be grateful to researchers willing to contribute examples of Golgi morphology (electron and light micrographs) in tissues, species or phyla not covered by the present report. To this purpose, please contact Francesco Ferraro at the following email addresses: francesco.ferraro@szn.it or f.ferraro.uk@gmail.com.

Author contributions

Conceptualization: F.F. Methodology: F.F., M.I.A., S.D., S.L. Investigation: F.F., G.B., S.L., E.A., S.Bo. Resources: S.J., M.K., K.M., V.H., V.B., H.E., S.Be., C.L., J.U-L., B.S., P.B., I.R-T., G.J., E.D. Writing original draft: F.F. Review & Editing: F.F., G.B., S.L., H.E., S.Be, S.D, J.U-L., C.L., I.R-T., B.S., G.J., P.B., M.I.A.. Visualization: F.F. Supervision: F.F.

Declaration of interests

The authors declare no competing interests

Figure titles and legends

Figure 1. Deuterostomes assemble Golgi ribbons. (A) Embryos of the sea urchin *Paracentrotus lividus* expressing fluorescent reporters of the Golgi apparatus and the plasma membrane (PM) were imaged at the indicated stages (hpf, hours post-fertilization; VEB, very early blastula; PHB, post-hatching blastula; BG, blastopore gastrula) by bright field and confocal microscopy (maximum intensity projections); right panels show magnifications of the middle panel insets; scale bars: 20 µm. (B) Maximum intensity projections of time-lapse confocal microscopy of an embryo microinjected as described in (A) and imaged at the indicated times (hpf); scale bar: 20 µm. (C) Number and size (median and interquartile range are shown) of Golgi objects in the embryo shown in (B) were measured; **, p <0.01; ****, p < 0.0001; Mann-Whitney test, compared to 8.5 hpf. (D)

Paracentrotus lividus, (E) *Ciona robusta* and (F) *Branchiostoma lanceolatum* embryos were processed for electron microscopy at the indicated developmental stages; Golgi elements are outlined (isolated stacks in light ochre; connected stacks in light magenta); scale bars: 1 µm. See also Figure S1 and Movie S1.

Figure 2. Golgi architecture in holozoans. The Golgi organization in holozoan exemplars from diverse taxa was analyzed at the ultrastructural level; separated and centralized stacks are highlighted in light ochre and light magenta, respectively. (A) The xenacoelomorph *Symsagittifera roscoffensis* (Roscoff worm), secretory cell. (B) The brachiopod *Calloria inconspicua*, epidermal cell of the mantle lobe of the three-lobed larva. (C) The annelid *Platynereis dumerilli*, glial cell of the 3-day old larva. (D) The crustacean *Parhyale hawaiensis*, nerve cell. (E) The jellyfish *Clytia hemisphaerica*, gonad gastrodermal cells. (F) The ctenophore *Mnemiopsis leydi:* epithelial cells. (G) The placozoan *Tricoplax adhaerens*. (H) The sea sponge *Oscarella carmela*, choanocyte. (I) The filasterean *Capsaspora owczarzaki.* Scale bars: 1 µm. (J) Deduced evolutionary emergence of the ribbon-like Golgi organization. Ribbon-like absence in both arthropods and nematodes, which both belong to the ecdysozoan superphylum, may indicate that loss of Golgi centralization occurred in their common ancestor. See also Figure S2 and Movie S2.

Figure 3. Putative molecular mediators of ribbon-like Golgi emergence. (A) The Golgi localized molecular tethers Golgins and GRASPs. Golgins are coiled-coil proteins that localize to Golgi membranes by a transmembrane region or through recruitment by small GTPases of the Arf, Arl and Rab families. Golgin localization within the stack (references[1,8,56,73,89]); their sizes (human homologs, bar length), and their evolutionary emergence[74] are indicated. (B) Evolution of GRASP-mediated Golgi stack tethering. In mammalian cells, dual anchoring of GRASPs on Golgi membranes is required for self-interaction in *trans* and stack tethering[12,16,17]. As GRASP myristoylation is ancestral (see text and Data S1A), we hypothesize that evolution of Golgin-45 binding to GRASP led to the emergence of stack linking and ribbon formation. (C) Solved structure (X-ray; PDB accession code 5H3J) and the AlphaFold2 (AF2) model of the mouse Golgin-45/GRASP complex. AF2 predicted structure almost overlaps the experimentally solved one (RMSD 3.040 Å for the Cα of the last 16 amino acids of the Golgin-45 C-terminal peptide). (D) AF2 models of holozoan GRASPs in complex with their conspecific Golgin-45 C-termini. Echinoderms, *Strongylocentrotus purpuratus*; annelids, *Platynereis dumerilii*; arthropods, *Drosophila melanogaster*; nematodes, *Caenorhabditis elegans*; mollusks, *Crassostrea gigas*; cnidarians, *Nematostella vectensis*; ctenophores, *Mnemiopsis leidyi*; placozoans, *Trichoplax adherens*; filastereans, *Capsaspora owczarzaki*. Altered conformations, with respect to the

mouse complex, are indicated by the arrows (blue for the PDZ-binding motif, red for the cysteine pair and green for the GRASP groove-interacting residues). (E) Deduced evolutionary appearance of GRASP binding by the C-terminus of Golgin-45 as deduced by AlphaFold2 modelling of holozoan complexes. See also Figure S3, S4 and Data S1.

STAR Methods

Key Resources Table

REAGENT or RESOURCE	SOURCE	IDENTIFIER
Antibodies		
Mouse monoclonal anti-GM130 (clone 35)	BD Biosciences	Cat# 610823
Bacterial strains		
One Shot™ TOP10 Chemically Competent *E. coli*	ThermoFisher	Cat# C404010
Chemicals		
DMSO, Hybri-Max™	Merck Millipore/Sigma-Aldrich	Cat# D2650
Nocodazole	Merck Millipore/Sigma-Aldrich	Cat# M1404
Critical commercial assays		
mMESSAGE mMACHINE T7 transcription kit	Invitrogen	Cat# AM1344
NEBuilder HiFi DNA assembly cloning kit	NEB	Cat# E5520
Q5® High-Fidelity DNA polymerase	NEB	Cat# M0491
Deposited data		
Experimental models: Cell lines		
Human Umbilical Vein Endothelial Cells (HUVECs) pooled donors	Promocell	Cat. No. C-12203
Experimental models: Organisms/strains		
Paracentrotus lividus – wild type	Gulf of Naples, Italy	N/A
Strongylocentrotus purpuratus – wild type	California, USA	N/A
Ciona robusta – wild type	Gulf of Taranto, Italy	N/A
Branchiostoma lanceolatum – wild type	Argelès-sur-mer, France	N/A
Platynereis dumerilii – wild type	Cultured colony (founders from the Gulf of Naples)	N/A
Calloria inconspicua – wild type	Karitane Point, New Zealand	N/A
Clytia hemisphaerica – wild type Z strain	Cultured colony Leclère et al 2019 doi.org/10.1038/s41559-019-0833-2	N/A
Symsagittifera roscoffensis – wild type	Roscoff, Brittany, France	N/A
Parhyale hawaiensis – wild type	Cultured colony (founders from the John G. Shedd Aquarium; Chicago; USA)	N/A
Trichoplax adhaerens – wild type	Cultured colony (founders from the Red Sea)	N/A
Mnemiopsis leidyi – wild type	Kristineberg, Sweden	N/A
Oscarella carmela – wild type	Carmel, California, USA	N/A

Capsaspora owczarzaki – wild type strain	Hertel, L.A., 2002 https://doi.org/10.1016/S0020-7519(02)00066-8	ATCC30864
Oligonucleotides		
Assembly primers for plasmid pCineo_mEGFP_Giant-CT Forward1: atacgactcactataggctagcATGGTGAGCAAGGGCGAG Reverse1: acctgatccaccgccCTTGTACAGCTCGTCCATGC Forward2: *ctgtacaag*ggcggtggatcaggtggaggatctACTCCTATCATTGGCTC Reverse2: gaggtaccacgcgtgaatTCATTACTATAGATGGCCC	This paper	N/A
Assembly primers for plasmid pCineo_GalT_mCherry Forward: ttaatacgactcactataggctagcATGAGGCTTCGGGAGCCG Reverse: ctctagaggtaccacgcgtgaattcTTACTTGTACAGCTCGTCCATGC	This paper	N/A
Assembly primers for plasmid pCineo_mCherry_CAAX Forward: ttaatacgactcactataggctagcATGGTGAGCAAGGGCGAG Reverse: ctctagaggtaccacgcgtg*aattcttacataattacacact ttgtctttgacttcttttcttcttttacc*CTTGTACAGCTCGTCCATGC	This paper	N/A
Recombinant DNA		
Plasmid: pCineo vector	Promega	Cat# E1841
Plasmid: pCineo_mEGFP_Giant-CT	This paper	N/A
Plasmid: pCineo_mCherry_CAAX	This paper	N/A
Plasmid: pCineo_GalT_mCherry	This paper	N/A
Software and algorithms		
ImageJ	Schindelin, J. et al. 2012 https://doi.org/10.1038/nmeth.2019	https://imagej.net/ij/index.html
Prism v9.4.1	N/A	https://www.graphpad.com/
BLAST	N/A	https://blast.ncbi.nlm.nih.gov/Blast.cgi

CLUSTAL-omega	Sievers, F. et al., 2011 https://doi.org/10.1038/msb.2011.75	https://www.ebi.ac.uk/Tools/msa/clustalo/
AliView	Larsson, A., 2014 https://doi.org/10.1093/bioinformatics/btu531	https://ormbunkar.se/aliview/
JalView	Waterhouse, A.M. et al., 2009 https://doi.org/10.1093/bioinformatics/btp033	https://www.jalview.org/
AlphaFold2	Jumper, J. et al., 2021 DOI: 10.1038/s41586-021-03819-2.	https://www.deepmind.com/open-source/alphafold
ColabFold	Mirdita, M. et al., 2022 https://doi.org/10.1038/s41592-022-01488-1	https://colab.research.google.com/github/sokrypton/ColabFold/blob/main/AlphaFold2.ipynb
Chimera	Pettersen E.F. et. al., 2004 https://doi.org/10.1002/jcc.20084	http://www.cgl.ucsf.edu/chimera/
NEBuilder	N/A	https://nebuilder.neb.com/

Method Details

Complex modelling. Models of complexes between conspecific GRASP/Golgin-45 pairs were built with the Colab implementation of AlphaFold2[77], using MMseqs2 to generate multiple sequences alignments[90]. To obtain reliable predictions of the protein-peptide complexes, AlphaFold-Multimer version v2 was used, with 12 recycles for the generation of each model[91]. Complexes were built without the use of structural templates and without Amber refinement as this step does not introduce substantial improvement, while significantly increasing computational time.

Further information regarding animals and experimental procedures is provided in the Supplemental Method details

Information about figures. Whether sponges or ctenophores or placozoans are the sister group to all other animals remains an unsettled issue[92-102]; for this reason the holozoan tree of life was drawn as a polytomy of these three taxa in the Graphical Abstract and Figures 2 and 3. The animal silhouettes used in the Graphical Abstract were obtained from the public domain (http://phylopic.org), when not covered by copyright, or drawn by F.F.

Resource availability

Materials availability

All reagents generated in this study are available from the lead contact upon request.

Data and code availability

All data reported in this paper will be shared by the lead contact upon request.

This paper does not report original code.

References

1. Tie, H.C., Ludwig, A., Sandin, S., and Lu, L. (2018). The spatial separation of processing and transport functions to the interior and periphery of the Golgi stack. Elife *7*. 10.7554/eLife.41301.

2. Cole, N.B., Sciaky, N., Marotta, A., Song, J., and Lippincott-Schwartz, J. (1996). Golgi dispersal during microtubule disruption: regeneration of Golgi stacks at peripheral endoplasmic reticulum exit sites. Molecular biology of the cell *7*, 631-650.

3. Wei, J.H., and Seemann, J. (2010). Unraveling the Golgi ribbon. Traffic (Copenhagen, Denmark) *11*, 1391-1400.

4. Mazzarello, P., Garbarino, C., and Calligaro, A. (2009). How Camillo Golgi became "the Golgi". FEBS Lett *583*, 3732-3737. 10.1016/j.febslet.2009.10.018.

5. Wei, J.H., and Seemann, J. (2017). Golgi ribbon disassembly during mitosis, differentiation and disease progression. Curr Opin Cell Biol *47*, 43-51. 10.1016/j.ceb.2017.03.008.

6. Gosavi, P., and Gleeson, P.A. (2017). The Function of the Golgi Ribbon Structure - An Enduring Mystery Unfolds! Bioessays *39*. 10.1002/bies.201700063.

7. Makhoul, C., Gosavi, P., and Gleeson, P.A. (2019). Golgi Dynamics: The Morphology of the Mammalian Golgi Apparatus in Health and Disease. Frontiers in cell and developmental biology *7*, 112. 10.3389/fcell.2019.00112.

8. Kulkarni-Gosavi, P., Makhoul, C., and Gleeson, P.A. (2019). Form and function of the Golgi apparatus: scaffolds, cytoskeleton and signalling. FEBS Lett *593*, 2289-2305. 10.1002/1873-3468.13567.

9. Saraste, J., and Prydz, K. (2019). A New Look at the Functional Organization of the Golgi Ribbon. Frontiers in cell and developmental biology *7*, 171. 10.3389/fcell.2019.00171.

10. Puthenveedu, M.A., Bachert, C., Puri, S., Lanni, F., and Linstedt, A.D. (2006). GM130 and GRASP65-dependent lateral cisternal fusion allows uniform Golgi-enzyme distribution. Nat Cell Biol *8*, 238-248. 10.1038/ncb1366.

11. Feinstein, T.N., and Linstedt, A.D. (2008). GRASP55 regulates Golgi ribbon formation. Molecular biology of the cell *19*, 2696-2707. 10.1091/mbc.E07-11-1200.

12. Sengupta, D., Truschel, S., Bachert, C., and Linstedt, A.D. (2009). Organelle tethering by a homotypic PDZ interaction underlies formation of the Golgi membrane network. The Journal of cell biology *186*, 41-55. 10.1083/jcb.200902110.

13. Truschel, S.T., Sengupta, D., Foote, A., Heroux, A., Macbeth, M.R., and Linstedt, A.D. (2011). Structure of the membrane-tethering GRASP domain reveals a unique PDZ ligand interaction that mediates Golgi biogenesis. The Journal of biological chemistry *286*, 20125-20129. 10.1074/jbc.C111.245324.

14. Grond, R., Veenendaal, T., Duran, J.M., Raote, I., van Es, J.H., Corstjens, S., Delfgou, L., El Haddouti, B., Malhotra, V., and Rabouille, C. (2020). The function of GORASPs in Golgi apparatus organization in vivo. The Journal of cell biology *219*. 10.1083/jcb.202004191.

15. Zhang, Y., and Seemann, J. (2021). Rapid degradation of GRASP55 and GRASP65 reveals their immediate impact on the Golgi structure. The Journal of cell biology *220*. 10.1083/jcb.202007052.

16. Bachert, C., and Linstedt, A.D. (2010). Dual anchoring of the GRASP membrane tether promotes trans pairing. The Journal of biological chemistry *285*, 16294-16301. 10.1074/jbc.M110.116129.

17. Heinrich, F., Nanda, H., Goh, H.Z., Bachert, C., Losche, M., and Linstedt, A.D. (2014). Myristoylation restricts orientation of the GRASP domain on membranes and promotes membrane tethering. The Journal of biological chemistry *289*, 9683-9691. 10.1074/jbc.M113.543561.

18. Rambourg, A., and Clermont, Y. (1997). Three-dimensional structure of the Golgi apparatus in mammalian cells. In The Golgi Apparatus, E.G. Berger, and J. Roth, eds. (Birkhäuser, Basel), pp. 37-61. 10.1007/978-3-0348-8876-9_2.

19. Eldon, E.D., Montpetit, I.C., Nguyen, T., Decker, G., Valdizan, M.C., Klein, W.H., and Brandhorst, B.P. (1990). Localization of the sea urchin Spec3 protein to cilia and Golgi complexes of embryonic ectoderm cells. Genes Dev *4*, 111-122. 10.1101/gad.4.1.111.

20. Terasaki, M. (2000). Dynamics of the endoplasmic reticulum and golgi apparatus during early sea urchin development. Molecular biology of the cell *11*, 897-914.

21. Kondylis, V., van Nispen tot Pannerden, H.E., Herpers, B., Friggi-Grelin, F., and Rabouille, C. (2007). The golgi comprises a paired stack that is separated at G2 by modulation of the actin cytoskeleton through Abi and Scar/WAVE. Developmental cell *12*, 901-915.

22. Yano, H., Yamamoto-Hino, M., Abe, M., Kuwahara, R., Haraguchi, S., Kusaka, I., Awano, W., Kinoshita-Toyoda, A., Toyoda, H., and Goto, S. (2005). Distinct functional units of the Golgi complex in Drosophila cells. Proceedings of the National Academy of Sciences of the United States of America *102*, 13467-13472. 10.1073/pnas.0506681102.

23. Page, K.M., McCormack, J.J., Lopes-da-Silva, M., Patella, F., Harrison-Lavoie, K., Burden, J.J., Quah, Y.B., Scaglioni, D., Ferraro, F., and Cutler, D.F. (2022). Structure modeling hints at a granular organization of the Golgi ribbon. BMC biology *20*, 111. 10.1186/s12915-022-01305-3.

24. Ayala, I., Mascanzoni, F., and Colanzi, A. (2020). The Golgi ribbon: mechanisms of maintenance and disassembly during the cell cycle. Biochem Soc Trans *48*, 245-256. 10.1042/BST20190646.

25. Ayala, I., and Colanzi, A. (2022). Structural Organization and Function of the Golgi Ribbon During Cell Division. Frontiers in cell and developmental biology *10*, 925228. 10.3389/fcell.2022.925228.

26. Thyberg, J., and Moskalewski, S. (1985). Microtubules and the organization of the Golgi complex. Exp Cell Res *159*, 1-16.

27. Kiyonari, H., Kaneko, M., Abe, T., Shioi, G., Aizawa, S., Furuta, Y., and Fujimori, T. (2019). Dynamic organelle localization and cytoskeletal reorganization during preimplantation mouse embryo development revealed by live imaging of genetically encoded fluorescent fusion proteins. Genesis *57*, e23277. 10.1002/dvg.23277.

28. Lu, Z., Joseph, D., Bugnard, E., Zaal, K.J., and Ralston, E. (2001). Golgi complex reorganization during muscle differentiation: visualization in living cells and mechanism. Molecular biology of the cell *12*, 795-808.

29. Gunn, P.A., Gliddon, B.L., Londrigan, S.L., Lew, A.M., van Driel, I.R., and Gleeson, P.A. (2011). The Golgi apparatus in the endomembrane-rich gastric parietal cells exist as functional stable mini-stacks dispersed throughout the cytoplasm. Biology of the cell *103*, 559-572. 10.1042/BC20110074.

30. Koga, D., and Ushiki, T. (2006). Three-dimensional ultrastructure of the Golgi apparatus in different cells: high-resolution scanning electron microscopy of osmium-macerated tissues. Arch Histol Cytol *69*, 357-374. 10.1679/aohc.69.357.

31. Ramón y Cajal, S. (1903). Sobre la existencia de un aparato tubuliforme en el protoplasma de las células nerviosas y epiteliales de la lombriz de tierra. Boletín de la Sociedad Española de Historia Natural, 395-398.

32. Perroncito, A. (1910). Contributo allo studio della biologia cellulare – mitocondri, cromidii e apparato reticolare interno nelle cellule spermatiche. Memorie della R. Accademia dei Lincei; Classe di Scienze Fisiche, Matematiche e Naturali *VIII*, 226-261.

33. Mollenhauer, H.H., and Morre, D.J. (1998). The tubular network of the Golgi apparatus. Histochem Cell Biol *109*, 533-543. 10.1007/s004180050253.

34. Meek, G.A., and Bradbury, S. (1963). Localization of thiamine pyrophosphatase activity in the golgi apparatus of a mollusc, Helix aspersa. The Journal of cell biology *18*, 73-85. 10.1083/jcb.18.1.73.

35. Sato, M., Saegusa, K., Sato, K., Hara, T., Harada, A., and Sato, K. (2011). Caenorhabditis elegans SNAP-29 is required for organellar integrity of the

endomembrane system and general exocytosis in intestinal epithelial cells. Molecular biology of the cell *22*, 2579-2587. 10.1091/mbc.E11-04-0279.

36. Witte, K., Schuh, A.L., Hegermann, J., Sarkeshik, A., Mayers, J.R., Schwarze, K., Yates, J.R., 3rd, Eimer, S., and Audhya, A. (2011). TFG-1 function in protein secretion and oncogenesis. Nat Cell Biol *13*, 550-558. 10.1038/ncb2225.

37. Kuterbach, D.A., and Walcott, B. (1986). Iron-containing cells in the honey-bee (Apis mellifera). I. Adult morphology and physiology. J Exp Biol *126*, 375-387. 10.1242/jeb.126.1.375.

38. Griffiths, G.W., and Beck, S.D. (1975). Ultrastructure of pea aphid mycetocytes: evidence for symbiote secretion. Cell Tissue Res *159*, 351-367. 10.1007/BF00221782.

39. Rolls, M.M., Marquardt, M.T., Kielian, M., and Machamer, C.E. (1997). Cholesterol-independent targeting of Golgi membrane proteins in insect cells. Molecular biology of the cell *8*, 2111-2118. 10.1091/mbc.8.11.2111.

40. Van-Praët, M. (1985). Nutrition of Sea Anemones. Advances in Marine Biology *22*, 65-99. https://doi.org/10.1016/S0065-2881(08)60050-4.

41. Sachkova, M.Y., Nordmann, E.L., Soto-Angel, J.J., Meeda, Y., Gorski, B., Naumann, B., Dondorp, D., Chatzigeorgiou, M., Kittelmann, M., and Burkhardt, P. (2021). Neuropeptide repertoire and 3D anatomy of the ctenophore nervous system. Curr Biol *31*, 5274-5285 e5276. 10.1016/j.cub.2021.09.005.

42. Burkhardt, P., Medhus, A., Digel, L., Naumann, B., Soto-Àngel, J.J., Nordmann, E.-L., Sachkova, M.Y., and Kittelmann, M. (2022). Syncytial nerve net in a ctenophore sheds new light on the early evolution of nervous systems. bioRxiv, 2022.2008.2014.503905. 10.1101/2022.08.14.503905.

43. Romanova, D.Y., Varoqueaux, F., Daraspe, J., Nikitin, M.A., Eitel, M., Fasshauer, D., and Moroz, L.L. (2021). Hidden cell diversity in Placozoa: ultrastructural insights from Hoilungia hongkongensis. Cell Tissue Res *385*, 623-637. 10.1007/s00441-021-03459-y.

44. Laundon, D., Larson, B.T., McDonald, K., King, N., and Burkhardt, P. (2019). The architecture of cell differentiation in choanoflagellates and sponge choanocytes. PLoS biology *17*, e3000226. 10.1371/journal.pbio.3000226.

45. Burkhardt, P., Stegmann, C.M., Cooper, B., Kloepper, T.H., Imig, C., Varoqueaux, F., Wahl, M.C., and Fasshauer, D. (2011). Primordial neurosecretory apparatus identified in the choanoflagellate Monosiga brevicollis. Proceedings of the National Academy of Sciences of the United States of America *108*, 15264-15269. 10.1073/pnas.1106189108.

46. Harrisson, F.W., and De Vos, L. (1991). Porifera (Willey-Liss).

47. Miller, P.M., Folkmann, A.W., Maia, A.R., Efimova, N., Efimov, A., and Kaverina, I. (2009). Golgi-derived CLASP-dependent microtubules control Golgi organization and polarized trafficking in motile cells. Nat Cell Biol *11*, 1069-1080. 10.1038/ncb1920.

534 48. Yadav, S., Puthenveedu, M.A., and Linstedt, A.D. (2012). Golgin160 recruits the
535 dynein motor to position the Golgi apparatus. Developmental cell *23*, 153-165.
536 10.1016/j.devcel.2012.05.023.

537 49. Tang, D., Zhang, X., Huang, S., Yuan, H., Li, J., and Wang, Y. (2016). Mena-
538 GRASP65 interaction couples actin polymerization to Golgi ribbon linking.
539 Molecular biology of the cell *27*, 137-152. 10.1091/mbc.E15-09-0650.

540 50. Zilberman, Y., Alieva, N.O., Miserey-Lenkei, S., Lichtenstein, A., Kam, Z., Sabanay,
541 H., and Bershadsky, A. (2011). Involvement of the Rho-mDia1 pathway in the
542 regulation of Golgi complex architecture and dynamics. Molecular biology of the cell
543 *22*, 2900-2911. 10.1091/mbc.E11-01-0007.

544 51. Makhoul, C., Gosavi, P., Duffield, R., Delbridge, B., Williamson, N.A., and Gleeson,
545 P.A. (2019). Intersectin-1 interacts with the golgin GCC88 to couple the actin
546 network and Golgi architecture. Molecular biology of the cell *30*, 370-386.
547 10.1091/mbc.E18-05-0313.

548 52. Kage, F., Steffen, A., Ellinger, A., Ranftler, C., Gehre, C., Brakebusch, C., Pavelka,
549 M., Stradal, T., and Rottner, K. (2017). FMNL2 and -3 regulate Golgi architecture
550 and anterograde transport downstream of Cdc42. Sci Rep *7*, 9791. 10.1038/s41598-
551 017-09952-1.

552 53. Gordon, D.E., Bond, L.M., Sahlender, D.A., and Peden, A.A. (2010). A targeted
553 siRNA screen to identify SNAREs required for constitutive secretion in mammalian
554 cells. Traffic (Copenhagen, Denmark) *11*, 1191-1204. 10.1111/j.1600-
555 0854.2010.01087.x.

556 54. Bailey Blackburn, J., Pokrovskaya, I., Fisher, P., Ungar, D., and Lupashin, V.V.
557 (2016). COG Complex Complexities: Detailed Characterization of a Complete Set of
558 HEK293T Cells Lacking Individual COG Subunits. Frontiers in cell and
559 developmental biology *4*, 23. 10.3389/fcell.2016.00023.

560 55. Liu, S., and Storrie, B. (2015). How Rab proteins determine Golgi structure.
561 International review of cell and molecular biology *315*, 1-22.
562 10.1016/bs.ircmb.2014.12.002.

563 56. Witkos, T.M., and Lowe, M. (2015). The Golgin Family of Coiled-Coil Tethering
564 Proteins. Frontiers in cell and developmental biology *3*, 86. 10.3389/fcell.2015.00086.

565 57. Short, B., Preisinger, C., Korner, R., Kopajtich, R., Byron, O., and Barr, F.A. (2001).
566 A GRASP55-rab2 effector complex linking Golgi structure to membrane traffic. The
567 Journal of cell biology *155*, 877-883. 10.1083/jcb.200108079.

568 58. Xiang, Y., and Wang, Y. (2010). GRASP55 and GRASP65 play complementary and
569 essential roles in Golgi cisternal stacking. The Journal of cell biology *188*, 237-251.
570 10.1083/jcb.200907132.

571 59. Bekier, M.E., 2nd, Wang, L., Li, J., Huang, H., Tang, D., Zhang, X., and Wang, Y.
572 (2017). Knockout of the Golgi stacking proteins GRASP55 and GRASP65 impairs
573 Golgi structure and function. Molecular biology of the cell *28*, 2833-2842.
574 10.1091/mbc.E17-02-0112.

575 60. Munro, S. (2011). The golgin coiled-coil proteins of the Golgi apparatus. Cold Spring
576 Harb Perspect Biol *3*. 10.1101/cshperspect.a005256.

577 61. Kinseth, M.A., Anjard, C., Fuller, D., Guizzunti, G., Loomis, W.F., and Malhotra, V.
578 (2007). The Golgi-associated protein GRASP is required for unconventional protein
579 secretion during development. Cell *130*, 524-534. 10.1016/j.cell.2007.06.029.

580 62. Zhang, X., Wang, L., Lak, B., Li, J., Jokitalo, E., and Wang, Y. (2018). GRASP55
581 Senses Glucose Deprivation through O-GlcNAcylation to Promote Autophagosome-
582 Lysosome Fusion. Developmental cell *45*, 245-261 e246.
583 10.1016/j.devcel.2018.03.023.

584 63. Nuchel, J., Tauber, M., Nolte, J.L., Morgelin, M., Turk, C., Eckes, B., Demetriades,
585 C., and Plomann, M. (2021). An mTORC1-GRASP55 signaling axis controls
586 unconventional secretion to reshape the extracellular proteome upon stress. Mol Cell
587 *81*, 3275-3293 e3212. 10.1016/j.molcel.2021.06.017.

588 64. Rabouille, C., and Linstedt, A.D. (2016). GRASP: A Multitasking Tether. Frontiers in
589 cell and developmental biology *4*, 1. 10.3389/fcell.2016.00001.

590 65. Barr, F.A., Puype, M., Vandekerckhove, J., and Warren, G. (1997). GRASP65, a
591 protein involved in the stacking of Golgi cisternae. Cell *91*, 253-262.

592 66. Shorter, J., Watson, R., Giannakou, M.E., Clarke, M., Warren, G., and Barr, F.A.
593 (1999). GRASP55, a second mammalian GRASP protein involved in the stacking of
594 Golgi cisternae in a cell-free system. The EMBO journal *18*, 4949-4960.
595 10.1093/emboj/18.18.4949.

596 67. Burd, C.G. (2021). GRASPing for consensus about the Golgi apparatus. The Journal
597 of cell biology *220*. 10.1083/jcb.202103117.

598 68. Kuo, A., Zhong, C., Lane, W.S., and Derynck, R. (2000). Transmembrane
599 transforming growth factor-alpha tethers to the PDZ domain-containing, Golgi
600 membrane-associated protein p59/GRASP55. The EMBO journal *19*, 6427-6439.
601 10.1093/emboj/19.23.6427.

602 69. Barr, F.A., Nakamura, N., and Warren, G. (1998). Mapping the interaction between
603 GRASP65 and GM130, components of a protein complex involved in the stacking of
604 Golgi cisternae. The EMBO journal *17*, 3258-3268. 10.1093/emboj/17.12.3258.

605 70. Malsam, J., Satoh, A., Pelletier, L., and Warren, G. (2005). Golgin tethers define
606 subpopulations of COPI vesicles. Science (New York, N.Y *307*, 1095-1098.
607 10.1126/science.1108061.

608 71. Wong, M., and Munro, S. (2014). Membrane trafficking. The specificity of vesicle
609 traffic to the Golgi is encoded in the golgin coiled-coil proteins. Science (New York,
610 N.Y *346*, 1256898. 10.1126/science.1256898.

611 72. Wong, M., Gillingham, A.K., and Munro, S. (2017). The golgin coiled-coil proteins
612 capture different types of transport carriers via distinct N-terminal motifs. BMC
613 biology *15*, 3. 10.1186/s12915-016-0345-3.

73. Lowe, M. (2019). The Physiological Functions of the Golgin Vesicle Tethering Proteins. Frontiers in cell and developmental biology *7*, 94. 10.3389/fcell.2019.00094.

74. Barlow, L.D., Nyvltova, E., Aguilar, M., Tachezy, J., and Dacks, J.B. (2018). A sophisticated, differentiated Golgi in the ancestor of eukaryotes. BMC biology *16*, 27. 10.1186/s12915-018-0492-9.

75. Zhao, J., Li, B., Huang, X., Morelli, X., and Shi, N. (2017). Structural Basis for the Interaction between Golgi Reassembly-stacking Protein GRASP55 and Golgin45. The Journal of biological chemistry *292*, 2956-2965. 10.1074/jbc.M116.765990.

76. Jumper, J., Evans, R., Pritzel, A., Green, T., Figurnov, M., Ronneberger, O., Tunyasuvunakool, K., Bates, R., Zidek, A., Potapenko, A., et al. (2021). Highly accurate protein structure prediction with AlphaFold. Nature *596*, 583-589. 10.1038/s41586-021-03819-2.

77. Mirdita, M., Schutze, K., Moriwaki, Y., Heo, L., Ovchinnikov, S., and Steinegger, M. (2022). ColabFold: making protein folding accessible to all. Nat Methods *19*, 679-682. 10.1038/s41592-022-01488-1.

78. Guo, H.B., Perminov, A., Bekele, S., Kedziora, G., Farajollahi, S., Varaljay, V., Hinkle, K., Molinero, V., Meister, K., Hung, C., et al. (2022). AlphaFold2 models indicate that protein sequence determines both structure and dynamics. Sci Rep *12*, 10696. 10.1038/s41598-022-14382-9.

79. Tsaban, T., Varga, J.K., Avraham, O., Ben-Aharon, Z., Khramushin, A., and Schueler-Furman, O. (2022). Harnessing protein folding neural networks for peptide-protein docking. Nature communications *13*, 176. 10.1038/s41467-021-27838-9.

80. Tamarin, A., and Keller, P.J. (1972). An ultrastructural study of the byssal thread forming system in Mytilus. J Ultrastruct Res *40*, 401-416. 10.1016/s0022-5320(72)90110-4.

81. Mendes, L.F.S., Batista, M.R.B., Kava, E., Bleicher, L., Micheletto, M.C., and Costa-Filho, A.J. (2022). Resurrecting Golgi proteins to grasp Golgi ribbon formation and self-association under stress. Int J Biol Macromol *194*, 264-275. 10.1016/j.ijbiomac.2021.11.173.

82. Ladinsky, M.S., Mastronarde, D.N., McIntosh, J.R., Howell, K.E., and Staehelin, L.A. (1999). Golgi structure in three dimensions: functional insights from the normal rat kidney cell. The Journal of cell biology *144*, 1135-1149.

83. Cole, N.B.S., C.L.; Sciaky, N.; Terasaki, M.; Edidin, M.; Lippincott-Schwartz, J. (1996). Diffusional mobility of Golgi proteins in membranes of living cells. Science (New York, N.Y *273*, 797-801. 10.1126/science.273.5276.797

84. Mendes, L.F.S., Fontana, N.A., Reddy, S.T., Uversky, V.N., and Costa-Filho, A.J. (2020). The exquisite structural biophysics of the Golgi Reassembly and Stacking Proteins. Int J Biol Macromol *164*, 3632-3644. 10.1016/j.ijbiomac.2020.08.203.

652 85. Knoll, A.H. (2011). The Multiple Origins of Complex Multicellularity. Annual
653 Review of Earth and Planetary Sciences *39*, 217–239.
654 10.1146/annurev.earth.031208.100209.

655 86. Vildanova, M.S., Wang, W., and Smirnova, E.A. (2014). Specific organization of
656 Golgi apparatus in plant cells. Biochemistry (Mosc) *79*, 894-906.
657 10.1134/S0006297914090065.

658 87. Staehelin, L.A., and Kang, B.H. (2008). Nanoscale architecture of endoplasmic
659 reticulum export sites and of Golgi membranes as determined by electron
660 tomography. Plant Physiol *147*, 1454-1468. 10.1104/pp.108.120618.

661 88. Bracker, C.E.M., D.J.; Grove, S.N.; (1996). Structure, differentiation, and
662 multiplication of Golgi apparatus in fungal hyphae. Protoplasma *194*, 250-274.

663 89. Gillingham, A.K., and Munro, S. (2016). Finding the Golgi: Golgin Coiled-Coil
664 Proteins Show the Way. Trends Cell Biol *26*, 399-408. 10.1016/j.tcb.2016.02.005.

665 90. Steinegger, M., and Soding, J. (2017). MMseqs2 enables sensitive protein sequence
666 searching for the analysis of massive data sets. Nature biotechnology *35*, 1026-1028.
667 10.1038/nbt.3988.

668 91. Johansson-Akhe, I., and Wallner, B. (2022). Improving peptide-protein docking with
669 AlphaFold-Multimer using forced sampling. Front Bioinform *2*, 959160.
670 10.3389/fbinf.2022.959160.

671 92. Philippe, H., Derelle, R., Lopez, P., Pick, K., Borchiellini, C., Boury-Esnault, N.,
672 Vacelet, J., Renard, E., Houliston, E., Queinnec, E., et al. (2009). Phylogenomics
673 revives traditional views on deep animal relationships. Curr Biol *19*, 706-712.
674 10.1016/j.cub.2009.02.052.

675 93. Pisani, D., Pett, W., Dohrmann, M., Feuda, R., Rota-Stabelli, O., Philippe, H.,
676 Lartillot, N., and Worheide, G. (2015). Genomic data do not support comb jellies as
677 the sister group to all other animals. Proceedings of the National Academy of
678 Sciences of the United States of America *112*, 15402-15407.
679 10.1073/pnas.1518127112.

680 94. Feuda, R., Dohrmann, M., Pett, W., Philippe, H., Rota-Stabelli, O., Lartillot, N.,
681 Worheide, G., and Pisani, D. (2017). Improved Modeling of Compositional
682 Heterogeneity Supports Sponges as Sister to All Other Animals. Curr Biol *27*, 3864-
683 3870 e3864. 10.1016/j.cub.2017.11.008.

684 95. Simion, P., Philippe, H., Baurain, D., Jager, M., Richter, D.J., Di Franco, A., Roure,
685 B., Satoh, N., Queinnec, E., Ereskovsky, A., et al. (2017). A Large and Consistent
686 Phylogenomic Dataset Supports Sponges as the Sister Group to All Other Animals.
687 Curr Biol *27*, 958-967. 10.1016/j.cub.2017.02.031.

688 96. Redmond, A.K., and McLysaght, A. (2021). Evidence for sponges as sister to all other
689 animals from partitioned phylogenomics with mixture models and recoding. Nature
690 communications *12*, 1783. 10.1038/s41467-021-22074-7.

97. Ryan, J.F., Pang, K., Schnitzler, C.E., Nguyen, A.D., Moreland, R.T., Simmons, D.K., Koch, B.J., Francis, W.R., Havlak, P., Program, N.C.S., et al. (2013). The genome of the ctenophore Mnemiopsis leidyi and its implications for cell type evolution. Science (New York, N.Y *342*, 1242592. 10.1126/science.1242592.

98. Moroz, L.L., Kocot, K.M., Citarella, M.R., Dosung, S., Norekian, T.P., Povolotskaya, I.S., Grigorenko, A.P., Dailey, C., Berezikov, E., Buckley, K.M., et al. (2014). The ctenophore genome and the evolutionary origins of neural systems. Nature *510*, 109-114. 10.1038/nature13400.

99. Borowiec, M.L., Lee, E.K., Chiu, J.C., and Plachetzki, D.C. (2015). Extracting phylogenetic signal and accounting for bias in whole-genome data sets supports the Ctenophora as sister to remaining Metazoa. BMC Genomics *16*, 987. 10.1186/s12864-015-2146-4.

100. Whelan, N.V., Kocot, K.M., Moroz, T.P., Mukherjee, K., Williams, P., Paulay, G., Moroz, L.L., and Halanych, K.M. (2017). Ctenophore relationships and their placement as the sister group to all other animals. Nat Ecol Evol *1*, 1737-1746. 10.1038/s41559-017-0331-3.

101. Laumer, C.E., Fernandez, R., Lemer, S., Combosch, D., Kocot, K.M., Riesgo, A., Andrade, S.C.S., Sterrer, W., Sorensen, M.V., and Giribet, G. (2019). Revisiting metazoan phylogeny with genomic sampling of all phyla. Proc Biol Sci *286*, 20190831. 10.1098/rspb.2019.0831.

102. Dellaporta, S.L., Xu, A., Sagasser, S., Jakob, W., Moreno, M.A., Buss, L.W., and Schierwater, B. (2006). Mitochondrial genome of Trichoplax adhaerens supports placozoa as the basal lower metazoan phylum. Proceedings of the National Academy of Sciences of the United States of America *103*, 8751-8756. 10.1073/pnas.0602076103.

Graphical abstract

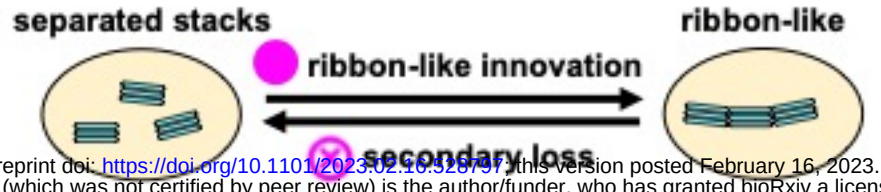

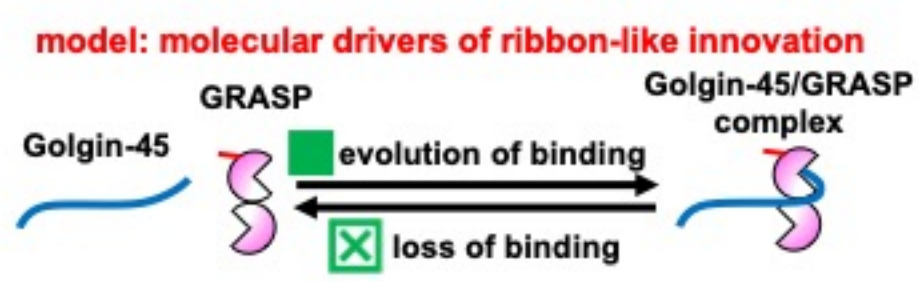

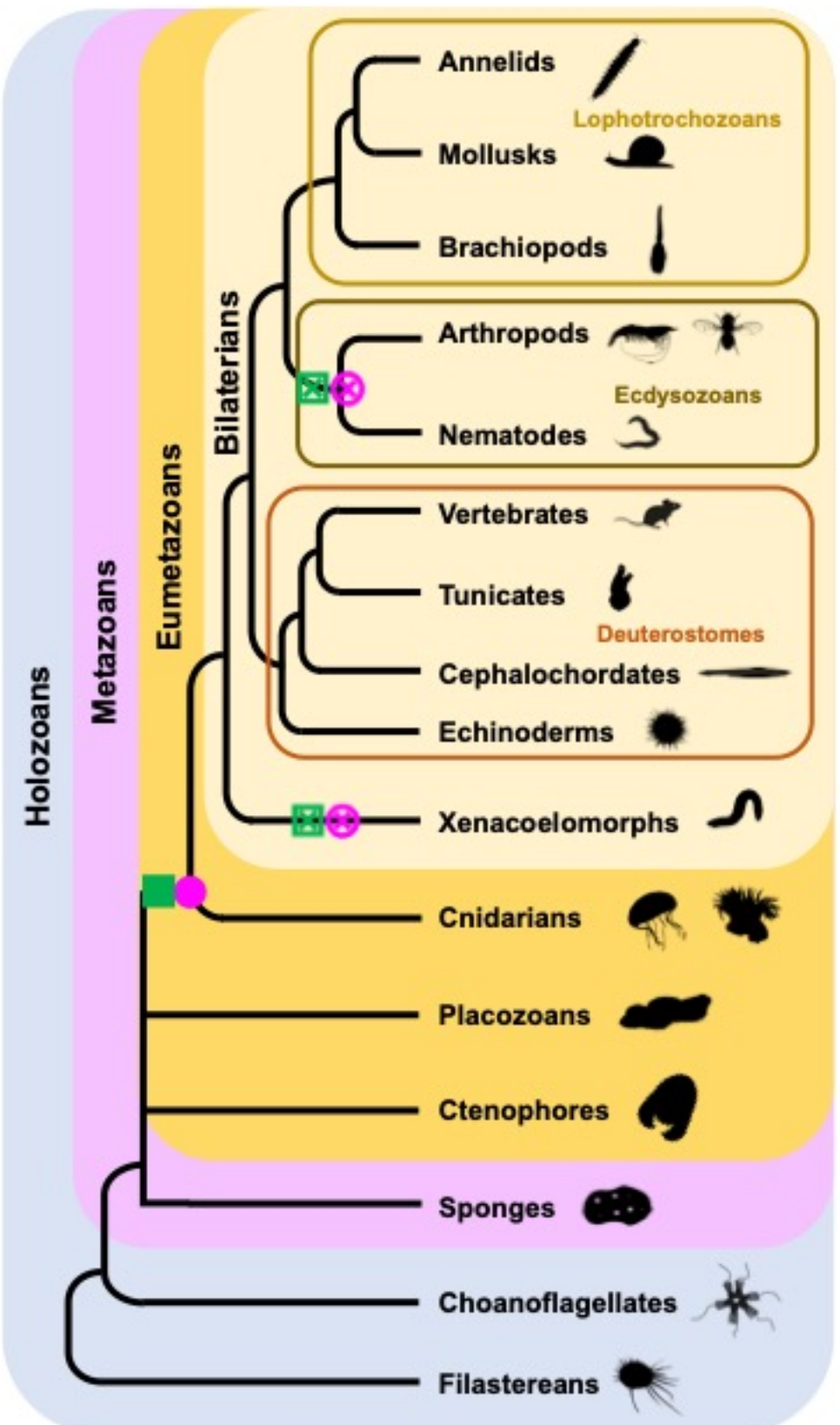

Figure 1

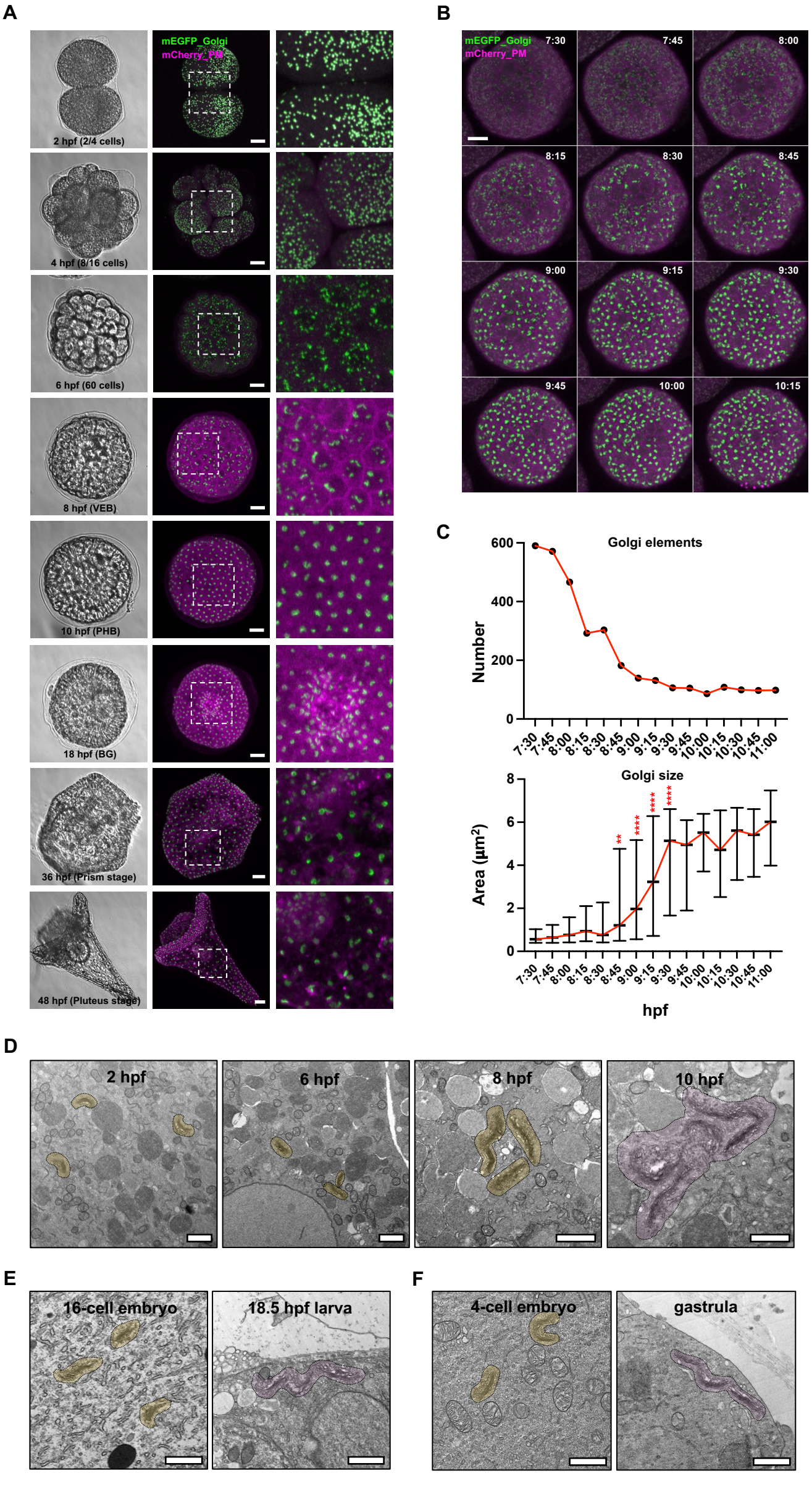
A
mEGFP_Golgi
mCherry_PM
2 hpf (2/4 cells)
4 hpf (8/16 cells)
6 hpf (60 cells)
8 hpf (VEB)
10 hpf (PHB)
18 hpf (BG)
36 hpf (Prism stage)
48 hpf (Pluteus stage)
B
mEGFP_Golgi
mCherry_PM
7:30
7:45
8:00
8:15
8:30
8:45
9:00
9:15
9:30
9:45
10:00
10:15
C
Golgi elements
Number
600
400
200
0
7:30 7:45 8:00 8:15 8:30 8:45 9:00 9:15 9:30 9:45 10:00 10:15 10:30 10:45 11:00
Golgi size
Area (µm²)
8
6
4
2
0
**
****
****
****
hpf
D
2 hpf
6 hpf
8 hpf
10 hpf
E
16-cell embryo
18.5 hpf larva
F
4-cell embryo
gastrula

Figure 2

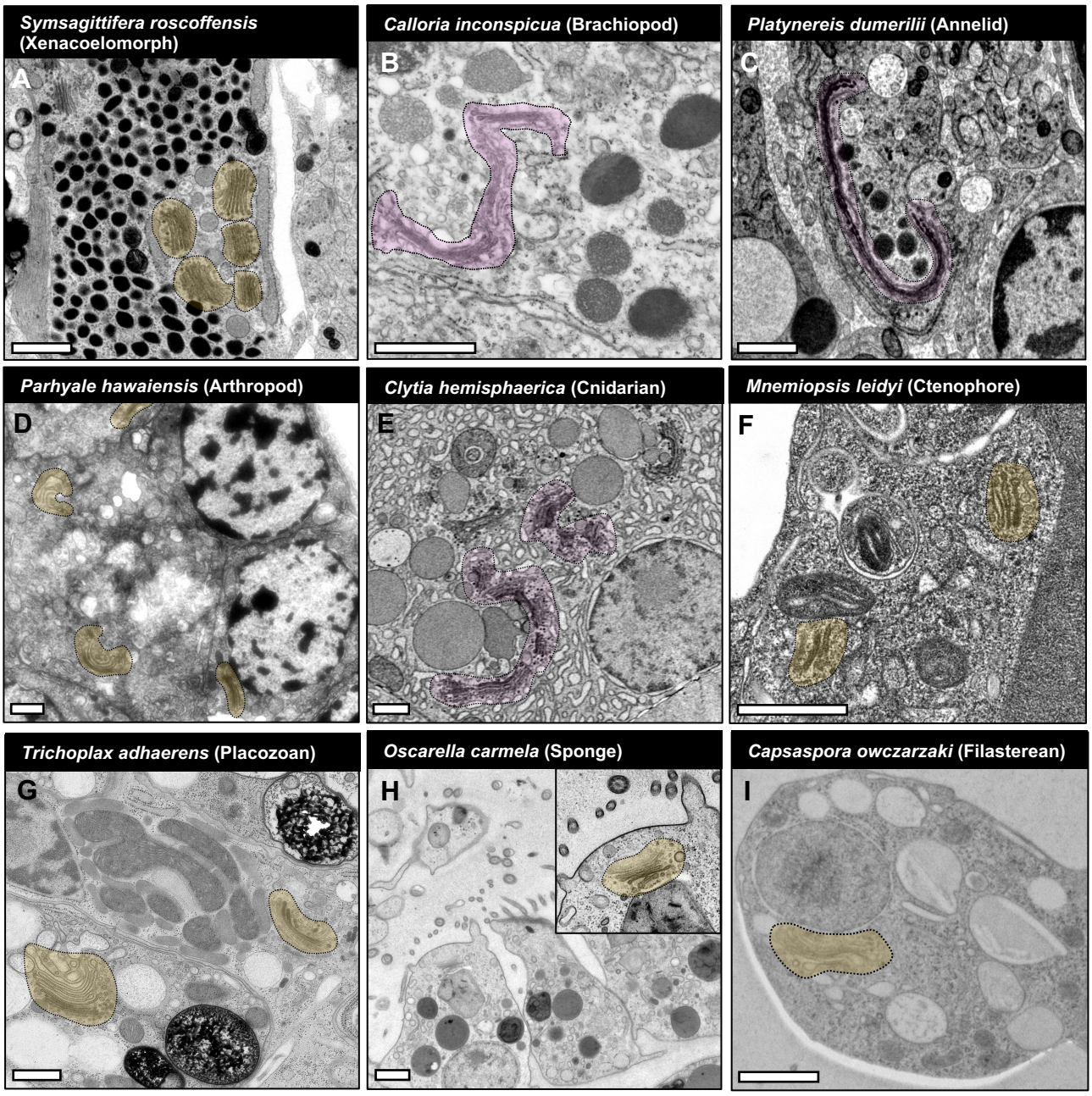
Symsagittifera roscoffensis (Xenacoelomorph)
A
Calloria inconspicua (Brachiopod)
B
Platynereis dumerilii (Annelid)
C
Parhyale hawaiensis (Arthropod)
D
Clytia hemisphaerica (Cnidarian)
E
Mnemiopsis leidyi (Ctenophore)
F
Trichoplax adhaerens (Placozoan)
G
Oscarella carmela (Sponge)
H
Capsaspora owczarzaki (Filasterean)
I

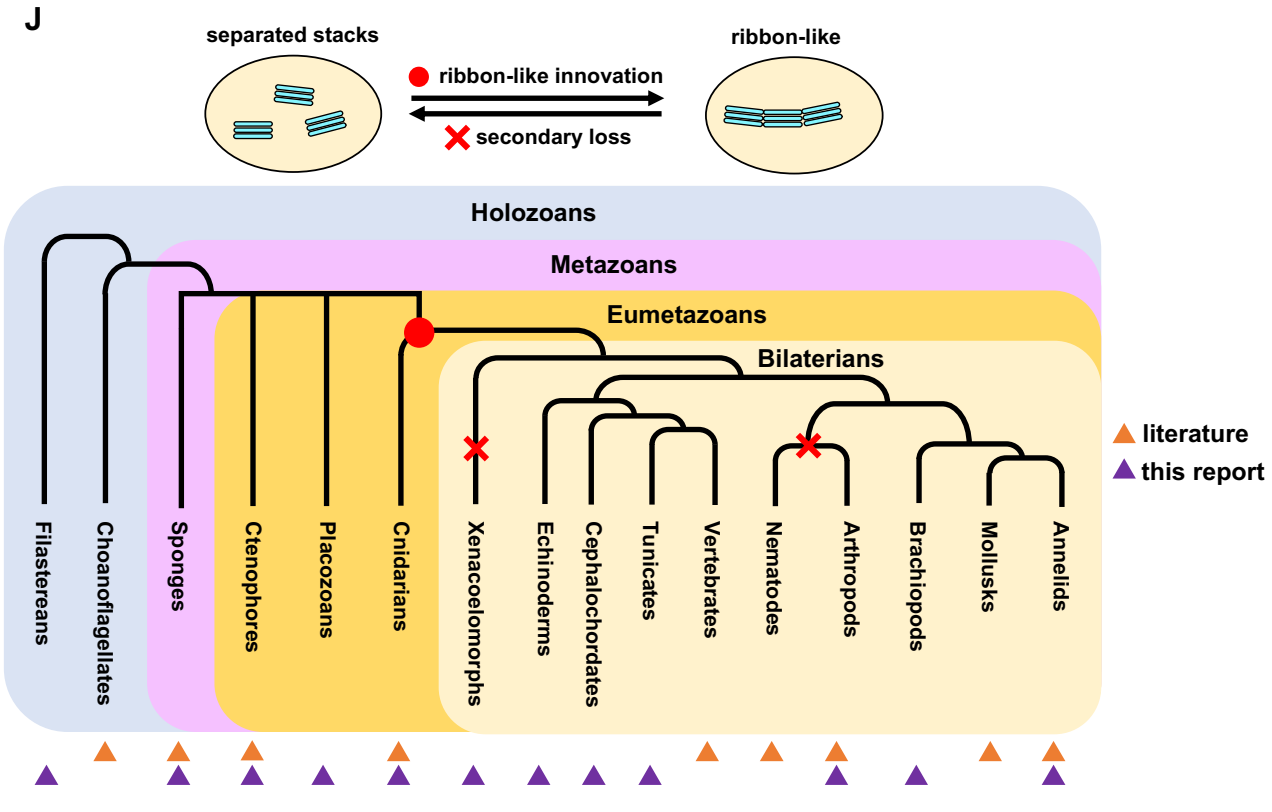
J
separated stacks
ribbon-like innovation
secondary loss
ribbon-like
Holozoans
Metazoans
Eumetazoans
Bilaterians
Filastereans
Choanoflagellates
Sponges
Ctenophores
Placozoans
Cnidarians
Xenacoelomorphs
Echinoderms
Cephalochordates
Tunicates
Vertebrates
Nematodes
Arthropods
Brachiopods
Mollusks
Annelids
literature
this report

Figure 3

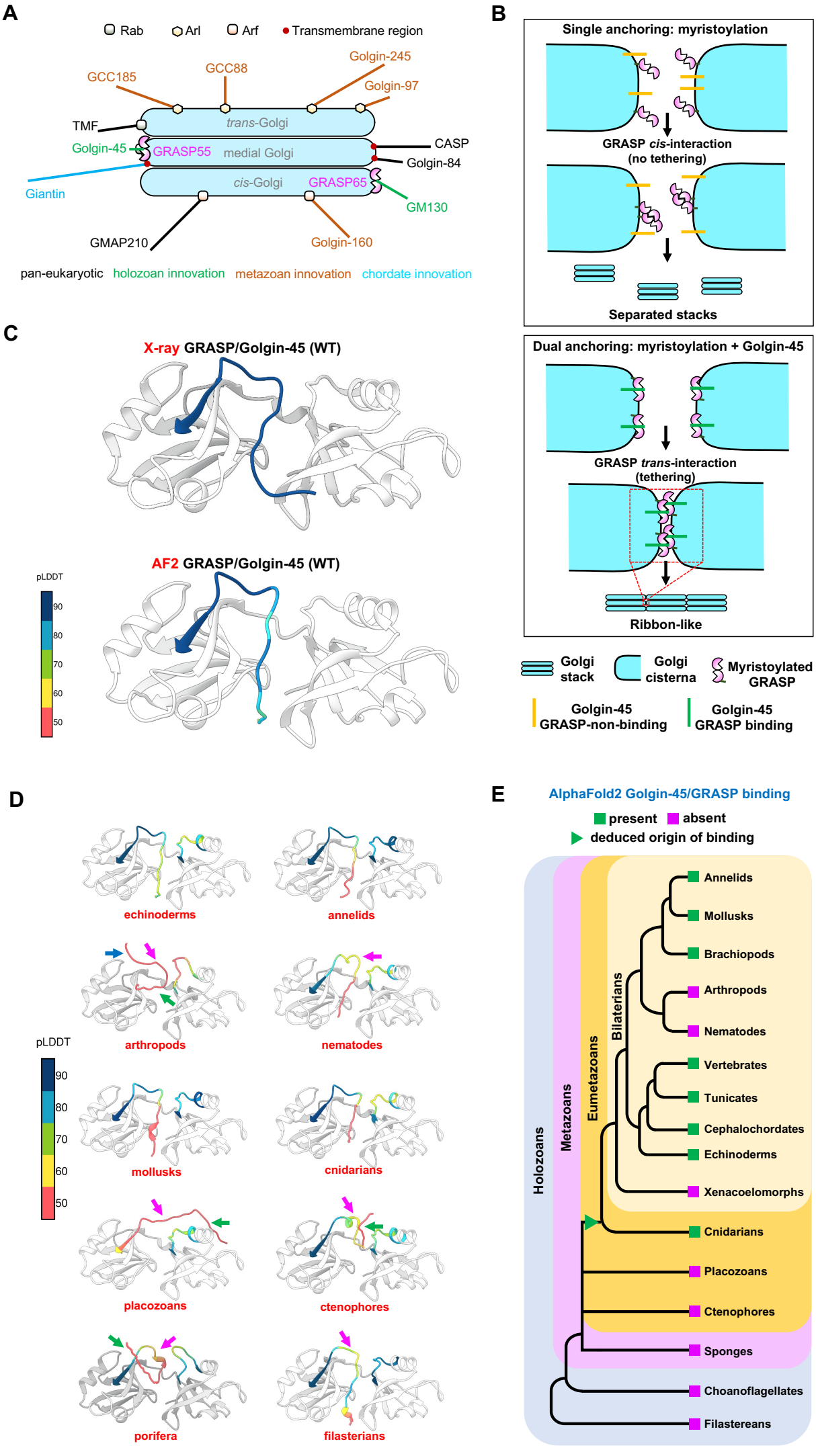
A
Rab
Arl
Arf
Transmembrane region
GCC185
GCC88
Golgin-245
Golgin-97
TMF
trans-Golgi
Golgin-45
GRASP55
medial Golgi
CASP
Golgin-84
Giantin
cis-Golgi
GRASP65
GM130
GMAP210
Golgin-160
pan-eukaryotic
holozoan innovation
metazoan innovation
chordate innovation
B
Single anchoring: myristoylation
GRASP cis-interaction
(no tethering)
Separated stacks
Dual anchoring: myristoylation + Golgin-45
GRASP trans-interaction
(tethering)
Ribbon-like
Golgi stack
Golgi cisterna
Myristoylated GRASP
Golgin-45 GRASP-non-binding
Golgin-45 GRASP binding
C
X-ray GRASP/Golgin-45 (WT)
AF2 GRASP/Golgin-45 (WT)
pLDDT
90
80
70
60
50
D
pLDDT
90
80
70
60
50
echinoderms
annelids
arthropods
nematodes
mollusks
cnidarians
placozoans
ctenophores
porifera
filasterians
E
AlphaFold2 Golgin-45/GRASP binding
present
absent
deduced origin of binding
Annelids
Mollusks
Brachiopods
Arthropods
Nematodes
Vertebrates
Tunicates
Cephalochordates
Echinoderms
Xenacoelomorphs
Cnidarians
Placozoans
Ctenophores
Sponges
Choanoflagellates
Filastereans
Bilaterians
Eumetazoans
Metazoans
Holozoans

Supplemental Information

Evolution of the ribbon-like organization of the Golgi apparatus in animal cells.

Authors
Giovanna Benvenuto, Serena Leone, Emanuele Astoricchio, Sophia Bormke, Sanja Jasek, Enrico D'Aniello, Maike Kittelmann, Kent McDonald, Volker Hartenstein, Valentina Baena, Héctor Escrivà, Stephanie Bertrand, Bernd Schierwater, Pawel Burkhardt, Iñaki Ruiz-Trillo, Gáspár Jékely, Jack Ullrich-Lüter, Carsten Lüter, Salvatore D'Aniello, Maria Ina Arnone, Francesco Ferraro

Supplemental Method Details

Experimental organisms. Animals were either sourced from the wild or lab cultured (see Key Resources table). Animal maintenance and treatments to obtain gametes for *in vitro* fertilization have been previously described[S1-7]. *Parhyale hawaiensis* embryos were a gift by Michalis Averof (Institut de Génomique Fonctionnelle de Lyon, IGFL). *Symsagittifera roscoffensis* juveniles, cultured at 15°C, were processed within 3 days of hatching. The *Capsaspora owczarzaki* ATCC30864 strain, established in 2002[S8]**,** was maintained in modified PYNFH medium (ATCC medium 1034) (https://www.atcc.org/products/327-x).

Cells. Human Umbilical Vein Endothelial Cells (HUVECs), expanded from pools of both sexes acquired from PromoCell, were maintained as described[S9] and used within the 4th passage.

Plasmids. Primers were designed using the NEBuilder tool (http://nebuilder.neb.com/). PCR reactions for amplicon generation were carried out with Q5 High-Fidelity DNA Polymerase (NEB). For primer sequences refer to the Key Resources table (KRT).
pCineo_mEGFP_Giant-CT (labelled in the figures as mEGFP_Golgi). The plasmid encodes mEGFP in frame with a linker sequence (GGGSGGGS) and the 69 C-terminal amino acids of human Giantin for Golgi membrane targeting. The mEGFP coding sequence was amplified from pmEGFP-N1 vector (Clontech) with primers forward 1 (lower case: pCineo sequence; upper case mEGFP coding sequence) and reverse 1 (lower case: GGGS coding sequence; upper case: mEGFP coding sequence). Refer to KRT.
The sequence encoding the 69 C-terminal amino acids of human Giantin was amplified from human umbilical vein endothelial cell (HUVEC) cDNA with primers forward 2 (italics: mEGFP coding sequence; lower case: GGGSGGGS linker coding sequence; upper case: Giantin

coding sequence) and reverse 2 (lower case: pCineo sequence; upper case: Giantin coding sequence and two stop codons). Refer to KRT.

pCineo_GalT_mCherry. A plasmid (the generous gift of Irina Kaverina, Vanderbilt School of Medicine) encoding the N-terminal 87 amino acids of galactosyl-transferase (GalT), which confer Golgi localization, in frame with mCherry[43] was used as template to amplify the GalT_mCherry coding sequence using primers forward (lower case: pCineo sequence; upper case: GatT coding sequence) and reverse (lower case: pCineo sequence; upper case: GatT coding sequence). Refer to KRT.

pCineo_mCherry_CAAX (labelled in the figures as mCherry_PM). The sequence encoding mCherry in frame with the polybasic sequence and CAAX motif of human K-Ras (GKKKKKKSKTKCVIM) for targeting to the plasma membrane was generated by amplification of mCherry using the pmCherry-N1 (Clontech) plasmid as template and the following primers: forward (lower case: pCineo sequence; upper case: mCherry coding sequence) and reverse (lower case: pCineo sequence; italics: polybasic plus CAAX motif and stop codon coding sequence; upper case: mCherry coding sequence). Refer to KRT.

Amplicons and pCineo plasmid (linearized by NheI/EcoRI digestion) were assembled using the NEBuilder HiFi DNA assembly cloning kit (NEB) following the manufacturer instructions. Correct sequences were verified by Sanger sequencing.

***In vitro* transcription**. Plasmids were linearized by digestion with NotI, a unique restriction site in the pCineo vector located downstream of the cloned sequences. One microgram of each linearized plasmid was used as template for *in vitro* transcription, using the mMESSAGE mMACHINE T7 transcription kit (ThermoFisher). Purified mRNAs were resuspended in DEPC-MilliQ water, their concentration measured**,** and their quality checked by agarose gel electrophoresis. mRNAs were aliquoted and stored at – 80°C until used.

mRNA microinjections. Sea urchin eggs' jelly coat was dissolved by a short wash in acidic filtered sea water (1.5 mM citric acid in 0.22 µm filtered sea water, FSW). De-jellied eggs were then immobilized on 60 mm plastic dish lids pre-treated with 1% protamine sulphate (Merck, Sigma-Aldrich, P4380) in FSW. Eggs were then washed with FSW containing sodium para-amino benzoate (Sigma-Aldrich, A6928; 0.05% in FSW) to prevent hardening of the fertilization envelope. *In vitro* transcribed mRNAs were diluted to a final concentration of 300-500 ng/µL in 120 mM KCl/DEPC-water. Four to five pL of diluted mRNAs were injected per embryo, immediately after fertilization. Embryos were allowed to develop at 18°C.

Confocal microscopy. *Paracentrotus lividus*. At the indicated times post-fertilization, embryo development was stopped by incubation with 0.2% paraformaldehyde in FSW, which kills the

embryos while preserving mEGFP and mCherry fluorescence. Imaging was carried out within 16 h of formaldehyde treatment. Embryos laid on glass-bottom dishes containing FSW were imaged with an inverted 25x (NA 0.8) water immersion objective, using a Zeiss LSM700 system. Image stacks (z-step 1 µm) were acquired. Only one third to one half of the embryo volumes could be imaged at early stages, due to the opacity of yolk granules. At later stages (prism and pluteus) embryos were transparent and their whole volume was imaged.

For live imaging experiments, eggs were laid in FWS containing glass-bottom dishes pre-treated with protamine, fertilized, and then immediately microinjected with fluorescent reporter encoding mRNAs. Imaging was carried out as described above. Image stacks (z-step 1 µm) were acquired at 15 min intervals. Higher magnification imaging of embryos was carried out on mEGFP_Giant-CT (mEGFP_Golgi) microinjected embryos using a 40x (NA 1.10) water immersion objective with a Leica SP8 confocal system. For presentation purposes, contrast-enhancement and gaussian-blur filtering were carried out (ImageJ) to the images shown.

HUVECs. Cells were seeded on gelatin-coated 96-well plates (Nunclon surface©, NUNC) at 15.000 cells/well and grown in HGM medium for 24 h. After rinsing with fresh medium, cells were fed HGM containing 0.1% (vol:vol) DMSO (control treatment) or 33 µM (10 mg/mL) Nocodazole and incubated for hours before fixation with 4% formaldehyde in phosphate-buffered saline (PBS) for 10 minutes at RT. Fixed cells were permeabilized with 0.2% TX-100 (Merck, Sigma-Aldrich) in PBS for 10 min (RT) and then blocked with 5% BSA (Merck, Sigma-Aldrich) in PBS for 30 min (RT). The Golgi apparatus was immuno-labeled with an antibody raised against the Golgi marker GM130 (BD Biosciences), followed by incubation with Alexa Fluor 488 conjugated anti-mouse antibody (Life Technologies); primary and secondary antibodies were diluted in 1% BSA/0.02% TX-100/PBS. Nuclei were counterstained with Hoechst 33342 (Life Technologies), diluted in PBS, and images acquired using an Opera High Content Screening System (Perkin Elmer) through a 40x air objective (NA 0.6).

Image analysis. Golgi objects from confocal images were analyzed with ImageJ (https://imagej.nih.gov/ij/). The Golgi channel (8-bit) was selected, maximum intensity projection images generated and processed as follows. Time course (Figure 1A). All images were subjected to background subtraction. Small Golgi objects observed at 2, 4 and 6 hpf were identified with the “find maxima” command and separated from each other by segmentation. The images of all time points were then subjected to thresholding and transformed into binary images. Golgi object number and size were then counted with the “analyze particles” command (area range was set at 0.25 – infinite μm^2). Three embryos per time point were analyzed. Time-lapse (Figure 1B). Image threshold was set automatically. At early time points, slight adjustments were done to correctly capture the size of most Golgi objects. For later time points, default threshold values were sufficient to correctly outline the

size Golgi objects. After transformation into binary images, object number and size were measured as described above. Numerical results were processed with Prism (Graphpad) for graph plotting and statistical analysis.

Electron microscopy. *Paracentrotus lividus*, *Branchiostoma lanceolatum* and *Ciona robusta* samples, maintained at 18°C, were collected at the indicated developmental stages and fixed at 4°C in 2% glutaraldehyde in filtered sea water (FSW). After fixation samples were first rinsed in FSW (6 x 10 min), then in Milli-Q water (3 x 10 min) and post-fixed with 1% osmium tetroxide and 1.5% potassium ferrocyanide (1 h, 4°C). Samples were then rinsed five times with Milli-Q water, dehydrated in a graded ethanol series, further substituted by propylene oxide and embedded in Epon 812 (TAAB, TAAB Laboratories Equipment Ltd, Berkshire, UK). Resin blocks were sectioned with a Ultracut UCT ultramicrotome (Leica, Vienna, Austria). Sections were placed on nickel grids and observed with a Zeiss LEO 912AB TEM (Zeiss, Oberkochen, Germany).

Calloria inconspicua. Three-lobed larvae were initially fixed in 2.5% glutardialdehyde buffered with 0.1 M sodium cacodylate solution (60 min at 5°C). A tiny amount ruthenium red solution was added to stain the extracellular matrix. Repeated rinsing in 0.1 M sodium cacodylate buffer was followed by post-fixation in 1% osmium tetroxide solution buffered with 0.1 M sodium cacodylate (40 min at 4°C). Dehydration with an acetone series and propylene oxide led to embedding in Araldite. Resin blocks were polymerized at 60°C for 48 hours. Ultrathin serial sections (70 nm) were cut on a Reichert Ultracut E microtome, placed on formvar-coated copper slot grids, and automatically stained with uranyl acetate and lead citrate in a LKB Ultrostainer. The sections were examined in Zeiss EM 10B and Zeiss EM 900 transmission electron microscopes.

Parhyale hawaiensis. Embryos were pre-fixed in 2.5% glutardialdehyde, 2% paraformaldehyde, 2% sucrose in sodium cacodylate buffer 0.1 M (SC buffer) overnight at 4°C. After several rinses in SC buffer at room temperature specimens were postfixed in 1% OsO4 in 0.1 M SC Buffer (2 hrs, room temperature), washed in SC buffer (1 hr) and dehydrated in an ethanol series. Ethanol-preserved specimens were sent to Berlin, transferred to 100% acetone and propylene oxide and subsequently embedded in araldite. Ultrathin sections were cut on a Leica EM UC7, stained with Plano uranyl acetate replacement stain (UAR-EMS) and lead citrate and investigated in a LEO EM 906.

Strongylocentrotus purpuratus, Platynereis dumerilii, *Mnemiopsis leidyi*, *Oscarella carmela* and *Capsaspora owczarzaki* samples were high-pressure frozen, freeze substituted and processed as described[S7,10-14].

Trichoplax adhaerens. Animals, alive of pre-fixed, were high-pressure frozen/freeze substituted and embedded in Epon. Sections (70 nm) were cut with using a Leica Ultracut UCT ultramicrotome.

Symsagittifera roscoffensis. Animals were processed within three days of hatching. The head of a hatchling was processed by high-pressure freezing. Freeze substitution was carried out in a solution of 1% osmium tetroxide and 0.1% uranyl acetate in acetone. A Leica Ultracut UCT was used to generate 60–80 nm sections, which were poststained in a 2% uranyl acetate/lead citrate solution and transferred to formvar-coated slit grids. Sections were imaged with a Tecnai 12 Biotwin TEM, using a fast-scan F214A CCD camera controlled by the SerialEM software (Boulder Lab). Digital image stacks were imported into the TrakEM2 package.

Clytia hemisphaerica. Individual ovaries were high-pressure frozen with a Wohlwend Compact 03 high-pressure freezing machine (http://www.wohlwend-hpf.ch) using sea water as the freezing medium and then transferred to a frozen solution of 2% osmium in acetone under liquid nitrogen. The ovaries were freeze-substituted in a Leica AFS2 freeze-substitution machine (https://www.leica-microsystems.com) using the following program: -90°C for 18 hours, -90°C to -30°C with a slope of 5°C/hour, -30°C for 12 hours, -30°C to 0°C with a slope of 5°C/hour. Samples were removed from the AFS chamber and allowed to reach room temperature. This was followed by 5 acetone washes for 5 minutes each. Ovaries were infiltrated with Polybed resin in a series of steps as follows: 1:3 resin to acetone overnight, 1:1 resin to acetone for 6 hours, 3:1 resin to acetone overnight, 100% resin for 6 hours followed by embedment in molds in fresh 100% resin and curation at 60°C for 2 days. Polymerized samples were then trimmed using an ultramicrotome to get the entire cross-section of the ovary. Serial 60 nm sections were collected using an Automated Tape-Collecting Ultramicrotome, mapped, and imaged with a Zeiss Sigma FE-SEM as described previously[S15].

Homology search. Canonical human GRASP (GRASP65 and GRASP55) and Golgin amino acid sequences (Data S1A) were used as initial queries. Homologs were searched in the target species using Basic Local Alignment Search Tool, BLAST, (BLASTp and TBLASTn) in available databases (Uniprot, NCBI, Ensembl). For specific target species, the search was carried out in dedicated databases (*Amphiura filiformis*: http://www.echinonet.org.uk/blast/; *Mnemiopsis leidyi*: https://research.nhgri.nih.gov/mnemiopsis/sequenceserver/; *Nematostella vectensis*: http://marimba.obs-vlfr.fr/blast; unicellular holozoans: https://protists.ensembl.org). Target genomes and, whenerver available, transcritpomes were interrogated. Hits with the lowest E-value and highest query coverage were selected as candidate homologs and validated when by reverse BLAST on the human proteome the query was retrieved as the

highest scoring. If this approach did not return a hit, homologs of evolutionarily closer species were used as queries. Further validation of homology was obtained by subjecting the hits to sequence and structural analysis with InterProScan (https://www.ebi.ac.uk/interpro/search/sequence/) and by multiple sequence alignment with AliView and JalView to verify regions of sequence similarity.

Supplemental Results and Discussion

Interpretation and predictive power of AlphaFold2 models. The introduction of AlphaFold[S16] and its subsequent evolutions produced a revolution in structural biology, allowing the obtainment of structure models of unprecedented accuracy. Recent benchmark studies have demonstrated that the predictive power of AF2 extends beyond the production of the mere structural models, yielding accurate results also for protein-protein and protein-peptide complexes, even when they imply conformational changes, and providing reliable hints on the effect of missense mutations[S17]. In the case of protein-peptide complexes, models with higher confidence can be obtained by increasing the number of recycles during model generation, provided that a sufficient number of sequences are detected during the generation of the multiple sequence alignments (MSAs)[S18,19]. In general, AF2 predicted models are evaluated and ranked based on a per residue score, the predicted local distance difference test (pLDDT). This value provides a measure, from a minimum of 0 to a maximum of 100, of the agreement between the prediction and experimental structures. Models or regions within them with an average pLDDT $\geq$ 70 are generally considered reliable[S20]. At the same time, it has been observed that low pLDDT values are indicative of intrinsically disordered regions and highly flexible stretches within proteins[S21,22]. Therefore, stable complexes, in which the binding partners have reduced mobility with respect to each other, are typically modelled with higher pLDDT scores. With all these considerations in mind, we built models for representative pairs of Golgin-45/GRASP from different species; the GRASPs from all species were modeled with extremely high confidence (average pLDDT $\geq$ 90), whereas variable results were obtained for the C-terminal peptides of the Golgins. In particular, peptides lacking the PDZ-binding motif (e.g., *D. melanogaster*) and/or the cysteines for Zn-finger formation (e.g., *M. leidyi*) could not adopt the binding conformation and were associated to very low pLDDT values. In general, lower pLDDT values characterized the residues interacting with the groove. While these scores could partially arise from low sequence coverage in the MSAs, they are also indicative of higher mobility of said regions, i.e., absence of interaction with the groove and, in some cases, complete displacement of the Golgin-45 peptide.

Role of groove residues in Golgin-45/GRASP interaction. To validate the structural conclusions derived from the crystal structure of the mouse GRASP domain (of GRASP55) in

complex with the Golgin-45 C-terminus, the authors of that study performed binding assays of protein mutants by pulldown experiments and isothermal titration calorimetry[S23]. Mutation of the last Golgin-45 residue (I403R), which disrupts the PDZ-binding, motif abolished binding to the GRASP domain; this was also the case when the cysteines involved in the Zinc finger formation were mutated (C393A, C3956A)[S23]. These results were correctly reproduced in AF2 models. In fact, as all modeled complexes have identical levels of sequence coverage, pLDDT decreases compared to the reference structure can in this case be ascribed to increased flexibility, decreased interaction, and reduced binding, and the displacement of the Golgin-45 peptide from its binding site is clearly visible in the structures obtained (compare Figure S4B and S4C to S4A). With respect to the interaction with the GRASP groove, the authors of the above study carried out binding assays with two Golgin-45 mutants, F390A and N391A, which did not abolish its interaction with the GRASP domain[S23]. From these results they concluded that the groove-binding residues of Golgin-45 play little or no role in GRASP interaction. However, the mutation of F390, which in the crystal structure is buried in the hydrophobic groove of the GRASP domain, to alanine is too conservative and should not impact groove binding. At the same time, the side chain of N391 in the crystal structure faces outwards from the GRASP groove, therefore also the mutation N391A is expected to have low impact on the interaction (Figure S3D). We modelled F390A and N391A mutations with AlphaFold2, finding, as expected, that they do not significantly alter the conformation of the Golgin-45 C-terminus and of the complex (Figure S4B). We conclude that these mutations are not ideal to assess the role of the interaction with the groove in the overall binding. For instance, replacement of F390 with a charged residue (F390R or F390E), which cannot be accommodated in the hydrophobic GRASP pocket, produced models devoid of the peptide/groove interaction and might be more indicated to experimentally validate the role of this interaction (Figure S4B). Of note, substitution of a charged residue in place of hydrophobic I388 (I388R) while making the region more flexible is still predicted to be able to fit the groove (Figure S4B), suggesting that some of the groove-inserting residues may be less important than others (e.g., F390) for the interaction with the GRASP domain. Although our modeling results may indicate that, at least in deuterostomes (with their highly conserved Golgin-45 and GRASP sequences), the Golgin-45 residues projecting into the GRASP groove increase binding stability, their actual contribution awaits experimental confirmation. Therefore, we considered stable binding between holozoan Golgin-45 and GRASP to occur when in their models both PDZ-binding motif interaction and Zinc finger formation were detected. It is worth noting that the conclusions regarding the appearance of Golgin-45/GRASP during evolution (Figure 3E) would not substantially change even in the case the Golgin-45 groove-interacting residues were shown to be required for GRASP binding (Figure 3D and S4A, green arrow).

Supplemental Figures

Figure S1. Golgi dynamics in the sea urchin embryo. Related to Figure 1. (A) The fluorescent reporter used in this study, mEGFP_Golgi, co-localizes with the widely used Golgi reporter GalT_mCherry; scale bar: 20 μm. (B) Quantification of Golgi object size (n = 3 embryos) from the time-course experiment shown in Figure 1A; ****, $p < 0.0001$ (Mann-Whitney test). (C) Golgi apparatus imaging of a 15 hpf *Paracentrotus lividus* embryo. A single focal plane acquired with a 40x water immersion objective is shown; scale bar: 5 μm. (D) *Paracentrotus lividus* embryos expressing the mEGFP_Golgi reporter imaged at the indicated stages; scale bar: 50 μm. (E) Observation of three or more stacks in close contact and/or with membrane continuities is the criterion adopted for positive identification of centralized Golgi in electron micrographs. (F) Golgi stacks a, b and c are seen establishing connections across serial sections (numbered in black), of a blastocoel cell of the sea urchin *Strongylocentrotus purpuratus* pluteus; scale bar: 1 μm. (G) Golgi disassembly/reassembly during mitosis in the *Paracentrotus lividus* embryo; image series (left to right, 15 min acquisition interval). Treatment with the microtubule depolymerizing compound nocodazole induces ribbon unlinking into constituent Golgi stacks in human umbilical vein endothelial cells, HUVECs, (H) and sea urchin embryos (I); magnifications of insets are shown; scale bars: 10 μm and 20 μm (HUVECs and sea urchin, respectively).

Figure S2. Additional examples of Golgi structure in holozoans. Related to Figure 2. (A) Golgi stack array in secretory cells of *Symsagittifera roscoffensis*. (B) A three-day-old *Platynereis dumerilii* larva. Serial sections (40 nm each), labelled starting from 1, are shown; in the region of interest, separated stacks (labelled a, b, c and d) in section 1 are seen to merge (c + d and then b + c + d) into a ribbon while progressing through the sections. (C) and (D) Two *Trichoplax adhaerens* cell types. (E) Comb cells of *Mnemiopsis leidyi*. Scale bars: 1 μm. (F) Table summarizing Golgi organization in species and cell types discussed in this report.

Figure S3. Structural features of holozoan GRASP and Golgin-45 proteins. Related to Figure 3. (A) Cartoon of domain structure of mammalian GRASPs. The evolutionarily conserved GRASP domain is formed by a tandem of atypical PDZ domains, followed by a C-terminal region, which in mammals is serine/proline-rich (SPR) and whose post-translational modifications modulate GRASP activity. (B) Size, in amino acids, of the GRASP domains and C-terminal regions of the holozoan GRASP sequences (Data S1A) were plotted; bars indicate median size. (C) Pairwise amino acid identity of holozoan GRASP domains plotted as a heat map. Vertebrate duplication into GRASP55 and GRASP65 paralogs occurred with the evolution of jawed vertebrates. In vertebrates, GRASP55 paralogs (green outlines) are more

similar to bilaterian single GRASPs than GRASP65 paralogs (red outlines); percent identity values for pairwise comparisons were obtained with CLUSTAL omega. (D) Structure of the GRASP domain (gold) of mouse GRASP55 in complex with the C-terminal residues of mouse Golgin-45 (ball and stick); PDB accession number 5H3J. PDZ1 and PDZ2 are indicated by color coded circles. Golgin-45 residues important for the interaction are highlighted; green, the stretch of residues interacting with the groove formed by PDZ1 and PDZ2 domains (arrows indicate F390 and N391, which are discussed in supplementary results and discussion and Figure S4); magenta, the two cysteines involved in Zinc-like finger formation; light blue, the PDZ-binding motif. (E) Multiple sequence alignment of the C-termini of the holozoan Golgin-45 homologs. The residues corresponding to the binding features are color coded as in S3D. Insertions (maroon highlight) and deletions (dashed boxes) are indicated relative to the mouse sequence; variations mostly affect the groove-binding sequence.

Figure S4. Additional AlphaFold2 models. Related to Figure 3. (A) Model of Golgin-45/GRASP complex in the only xenacoelomorph species with a Golgin-45 gene (Data S1B). (B) Models of mouse Golgin-45 mutants in complex with mouse GRASP domain; color-coded arrows indicate altered binding features as detailed in Figure 3D.

Supplemental video S1. Golgi clustering in the sea urchin embryo. Related to Figure 1. Time-lapse microscopy of Golgi element dynamics in a *Paracentrotus lividus* (shown as image series in Figure 1B). Maximum intensity projection of image stacks acquired at 15 min intervals between 7h:30m and 10h:15m post-fertilization are shown.

Supplemental video S2. Golgi ribbon in a glial cell of the three-day-old *Platynereis dumerilii* larva. Related to Figure 2. Image stack encompassing the image shown in Figure 2H.

Data S1. Holozoan GRASP and Golgin-45 homologs. Related to Figure 3. (A) GRASP homologs. GRASP domains, defined as residues number 1 to the fifth following the invariant motif His-Arg-Iso-Pro at the end of the second PDZ domain, are highlighted in bold; the conserved glycine residues in position 2 are highlighted in red. (B) Golgin-45 homologs. InterProScan analysis identified all the sequences as Golgin-45/BLZF1-like. In xenacoelomorphs, a Golgin-45 homolog was found only in *Hofstenia miamia*.

Supplemental References

S1. Paganos, P., Caccavale, F., La Vecchia, C., D'Aniello, E., D'Aniello, S., and Arnone, M.I. (2022). FISH for All: A Fast and Efficient Fluorescent In situ Hybridization

(FISH) Protocol for Marine Embryos and Larvae. Front Physiol *13*, 878062. 10.3389/fphys.2022.878062.

S2. Reed, C.G. (1987). Reproduction and development of marine invertebrates of the northern Pacific coast. Phylum Brachiopoda. (University of Washington Press), 486–493.

S3. Nislow, C. (1994). Reproduction and development of marine invertebrates. Cellular dynamics during the early development of an articulate brachiopod. (Johns Hopkins University Press,), 118-128.

S4. Schierwater, B. (2005). My favorite animal, Trichoplax adhaerens. Bioessays *27*, 1294-1302. 10.1002/bies.20320.

S5. Browne, W.E., Price, A.L., Gerberding, M., and Patel, N.H. (2005). Stages of embryonic development in the amphipod crustacean, Parhyale hawaiensis. Genesis *42*, 124-149. 10.1002/gene.20145.

S6. Leclere, L., Horin, C., Chevalier, S., Lapebie, P., Dru, P., Peron, S., Jager, M., Condamine, T., Pottin, K., Romano, S., et al. (2019). The genome of the jellyfish Clytia hemisphaerica and the evolution of the cnidarian life-cycle. Nat Ecol Evol *3*, 801-810. 10.1038/s41559-019-0833-2.

S7. Sachkova, M.Y., Nordmann, E.L., Soto-Angel, J.J., Meeda, Y., Gorski, B., Naumann, B., Dondorp, D., Chatzigeorgiou, M., Kittelmann, M., and Burkhardt, P. (2021). Neuropeptide repertoire and 3D anatomy of the ctenophore nervous system. Curr Biol *31*, 5274-5285 e5276. 10.1016/j.cub.2021.09.005.

S8. Hertel, L.A., Bayne, C.J., and Loker, E.S. (2002). The symbiont Capsaspora owczarzaki, nov. gen. nov. sp., isolated from three strains of the pulmonate snail Biomphalaria glabrata is related to members of the Mesomycetozoea. Int J Parasitol *32*, 1183-1191. 10.1016/s0020-7519(02)00066-8.

S9. Ferraro, F., Patella, F., Costa, J.R., Ketteler, R., Kriston-Vizi, J., and Cutler, D.F. (2020). Modulation of endothelial organelle size as an antithrombotic strategy. J Thromb Haemost. 10.1111/jth.15084.

S10. Paganos, P., Ronchi, P., Carl, J., Mizzon, G., Martinez, P., Benvenuto, G., and Arnone, M.I. (2022). Integrating single cell transcriptomics and volume electron microscopy confirms the presence of pancreatic acinar-like cells in sea urchins. Frontiers in cell and developmental biology *10*, 991664. 10.3389/fcell.2022.991664.

S11. Sebe-Pedros, A., Irimia, M., Del Campo, J., Parra-Acero, H., Russ, C., Nusbaum, C., Blencowe, B.J., and Ruiz-Trillo, I. (2013). Regulated aggregative multicellularity in a close unicellular relative of metazoa. Elife *2*, e01287. 10.7554/eLife.01287.

S12. Verasztó, C., Jasek, S., Gühmann, M., Shahidi, R., Ueda, N., Beard, J.D., Mendes, S., Heinz, K., Bezares-Calderón, L.A., Williams, E., and Jékely, G. (2020). Whole-animal connectome and cell-type complement of the three-segmented Platynereis dumerilii larva. biorXiv. https://doi.org/10.1101/2020.08.21.260984

S13. Laundon, D., Larson, B.T., McDonald, K., King, N., and Burkhardt, P. (2019). The architecture of cell differentiation in choanoflagellates and sponge choanocytes. PLoS biology *17*, e3000226. 10.1371/journal.pbio.3000226.

S14. Burkhardt, P., Medhus, A., Digel, L., Naumann, B., Soto-Àngel, J.J., Nordmann, E.-L., Sachkova, M.Y., and Kittelmann, M. (2022). Syncytial nerve net in a ctenophore sheds new light on the early evolution of nervous systems. bioRxiv, 2022.2008.2014.503905. 10.1101/2022.08.14.503905.

S15. Baena, V., Schalek, R.L., Lichtman, J.W., and Terasaki, M. (2019). Serial-section electron microscopy using automated tape-collecting ultramicrotome (ATUM). Methods in cell biology *152*, 41-67. 10.1016/bs.mcb.2019.04.004.

S16. Jumper, J., Evans, R., Pritzel, A., Green, T., Figurnov, M., Ronneberger, O., Tunyasuvunakool, K., Bates, R., Zidek, A., Potapenko, A., et al. (2021). Highly accurate protein structure prediction with AlphaFold. Nature *596*, 583-589. 10.1038/s41586-021-03819-2.

S17. Akdel, M., Pires, D.E.V., Pardo, E.P., Janes, J., Zalevsky, A.O., Meszaros, B., Bryant, P., Good, L.L., Laskowski, R.A., Pozzati, G., et al. (2022). A structural biology community assessment of AlphaFold2 applications. Nat Struct Mol Biol *29*, 1056-1067. 10.1038/s41594-022-00849-w.

S18. Tsaban, T., Varga, J.K., Avraham, O., Ben-Aharon, Z., Khramushin, A., and Schueler-Furman, O. (2022). Harnessing protein folding neural networks for peptide-protein docking. Nature communications *13*, 176. 10.1038/s41467-021-27838-9.

S19. Johansson-Akhe, I., and Wallner, B. (2022). Improving peptide-protein docking with AlphaFold-Multimer using forced sampling. Front Bioinform *2*, 959160. 10.3389/fbinf.2022.959160.

S20. Tunyasuvunakool, K., Adler, J., Wu, Z., Green, T., Zielinski, M., Zidek, A., Bridgland, A., Cowie, A., Meyer, C., Laydon, A., et al. (2021). Highly accurate protein structure prediction for the human proteome. Nature *596*, 590-596. 10.1038/s41586-021-03828-1.

S21. Guo, H.B., Perminov, A., Bekele, S., Kedziora, G., Farajollahi, S., Varaljay, V., Hinkle, K., Molinero, V., Meister, K., Hung, C., et al. (2022). AlphaFold2 models indicate that protein sequence determines both structure and dynamics. Sci Rep *12*, 10696. 10.1038/s41598-022-14382-9.

S22. Ruff, K.M., and Pappu, R.V. (2021). AlphaFold and Implications for Intrinsically Disordered Proteins. Journal of molecular biology *433*, 167208. 10.1016/j.jmb.2021.167208.

S23. Zhao, J., Li, B., Huang, X., Morelli, X., and Shi, N. (2017). Structural Basis for the Interaction between Golgi Reassembly-stacking Protein GRASP55 and Golgin45. The Journal of biological chemistry *292*, 2956-2965. 10.1074/jbc.M116.765990.

Figure S1

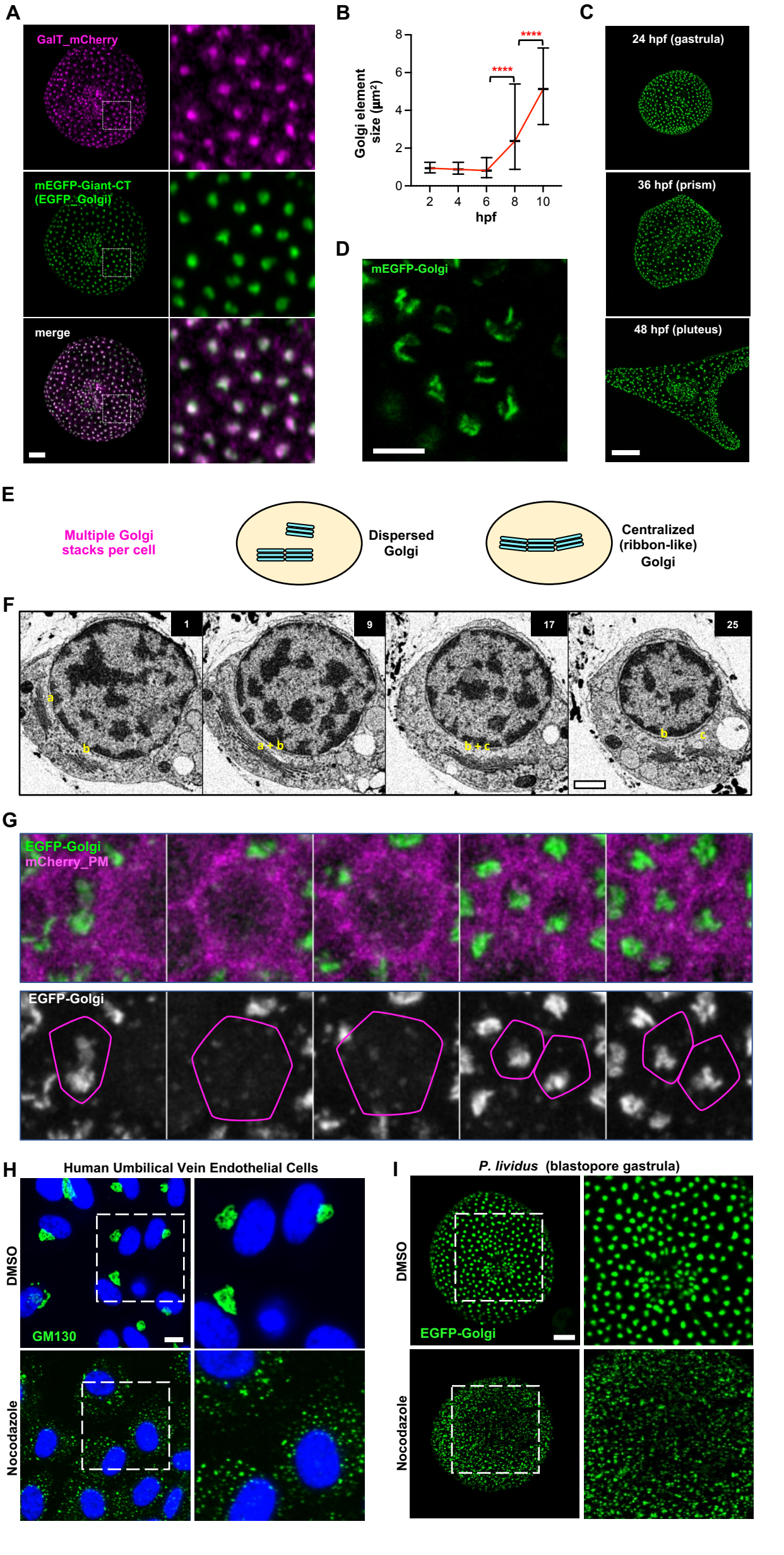
A
GalT_mCherry
mEGFP-Giant-CT
(EGFP_Golgi)
merge
B
Golgi element size (µm²)
hpf
****
****
C
24 hpf (gastrula)
36 hpf (prism)
48 hpf (pluteus)
D
mEGFP-Golgi
E
Multiple Golgi stacks per cell
Dispersed Golgi
Centralized (ribbon-like) Golgi
F
1
9
17
25
a
b
a + b
b + c
b
c
G
EGFP-Golgi
mCherry_PM
EGFP-Golgi
H
Human Umbilical Vein Endothelial Cells
DMSO
Nocodazole
GM130
I
P. lividus (blastopore gastrula)
DMSO
Nocodazole
EGFP-Golgi

Figure S2

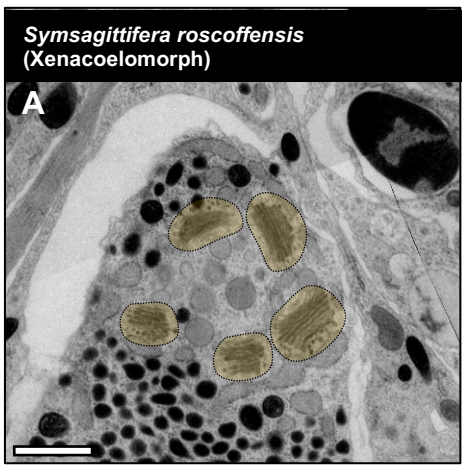

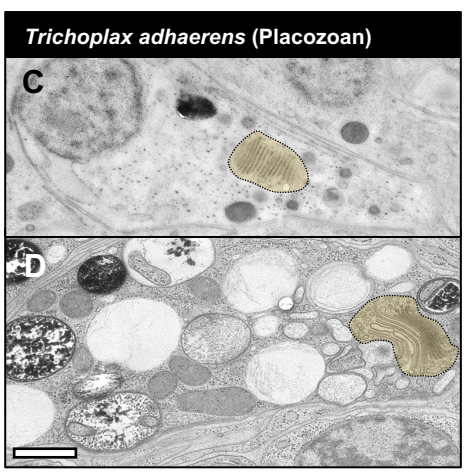

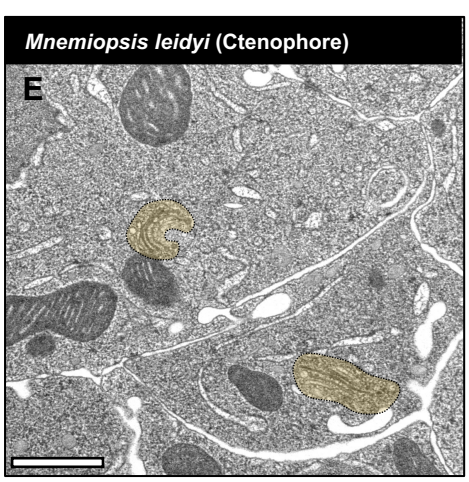

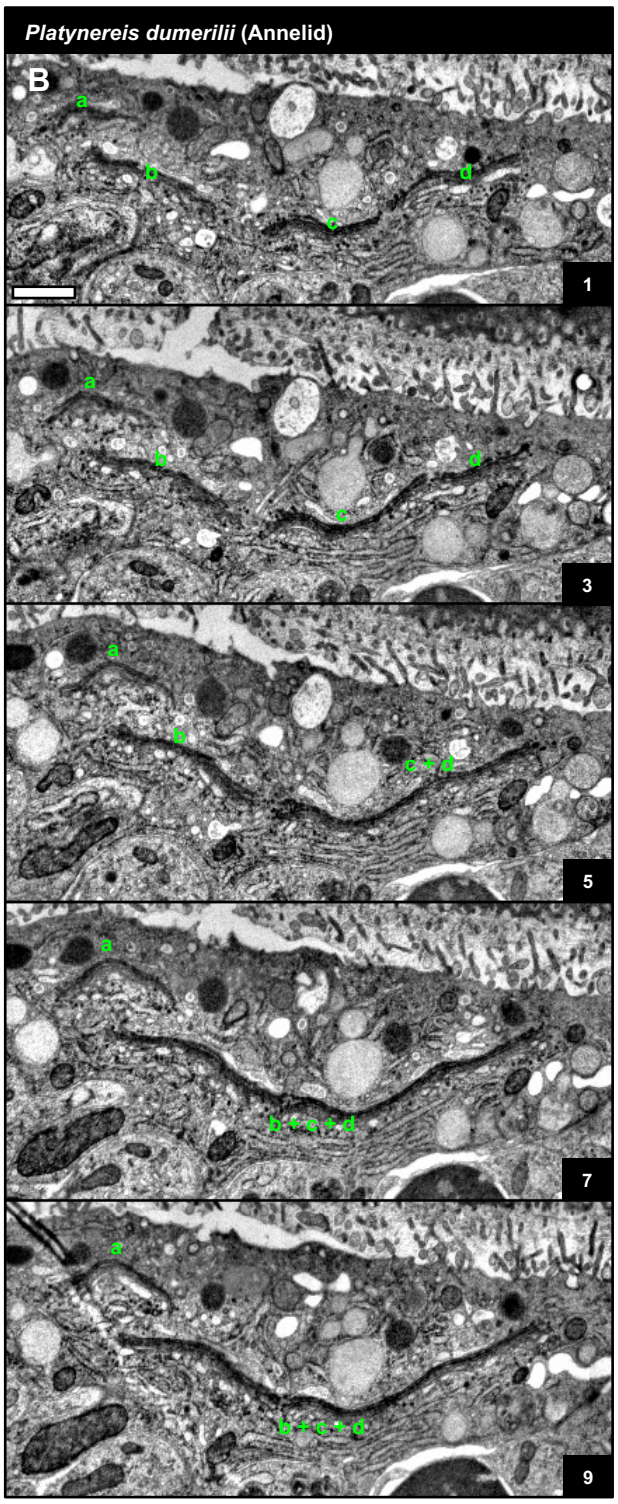

F

Species	Taxon	Multiple Golgi stacks per cell	Presence of ribbon-like Golgi	Source of morphological data	Tissues/cell types
C. robusta	Tunicates	+	+	This paper	epidermal cells of larva
B. lanceolatum	Cephalocordates	+	+	This paper	ectodermal cells of gastrula
S. purpuratus	Echinoderms	+	+	This paper	blastocoelar cells of pluteus larva
P. lividus	Echinoderms	+	+	This paper	all cells from pre-hatching blastula to pluteus larva
L. variegatus	Echinoderms	+	+	Literature	all cells in pre-hatching blastula
L. pictus	Echinoderms	+	+	Literature	all cells in blastula and prism stage
D. melanogaster	Arthropods	+	–	Literature	all cell types (larva and adult) and cell lines
A. mellifera	Arthropods	+	–	Literature	Trophocyte
A. pisum	Arthropods	+	–	Literature	Mycetocytes
A. albopictus	Arthropods	+	–	Literature	cell line
P. hawaiensis	Arthropods	+	–	This paper	all cell types (adult)
C. elegans	nematodes	+	–	Literature	all cell types
C. inconspicua	Brachiopods	+	–	This paper	epidermal cells of 3-lobe larva
P. vivipara	Mollusks	+	+	Literature	spermatocytes
H. pomatia	Mollusks	+	+	Literature	multified gland cells
H. aspersa	Mollusks	+	+	Literature	early spermatocytes
P. dumerilii	Annelids	+	+	This paper	several cell types of 3-day-old larva
Lumbricus (unreported species)	Annelids	+	+	Literature	epithelial cells and neurons of adult
S. roscoffensis	Xenacoelomorphs	+	+	This paper	secretory granule producing cells
C. hemisphaerica	Cnidarians	+	+	This paper	gastrodermal cells of adult
M. leidyi	Ctenophores	+	–	This paper	epithelial and comb cells
T. adhaerens	Placozoans	–	N/A	This paper	all cell types
H. hongkongensis	Placozoans	–	N/A	Literature	all cell types
O. carmela	Sponges	–	N/A	Literature and this paper	all cell types
E. fluviatilis	Sponges	+	–	Literature	spongocyte
S. rosetta	Choanoflagellates	–	N/A	Literature	N/A
C. owczarzaki	Filasterians	–	N/A	This paper	N/A

Figure S3

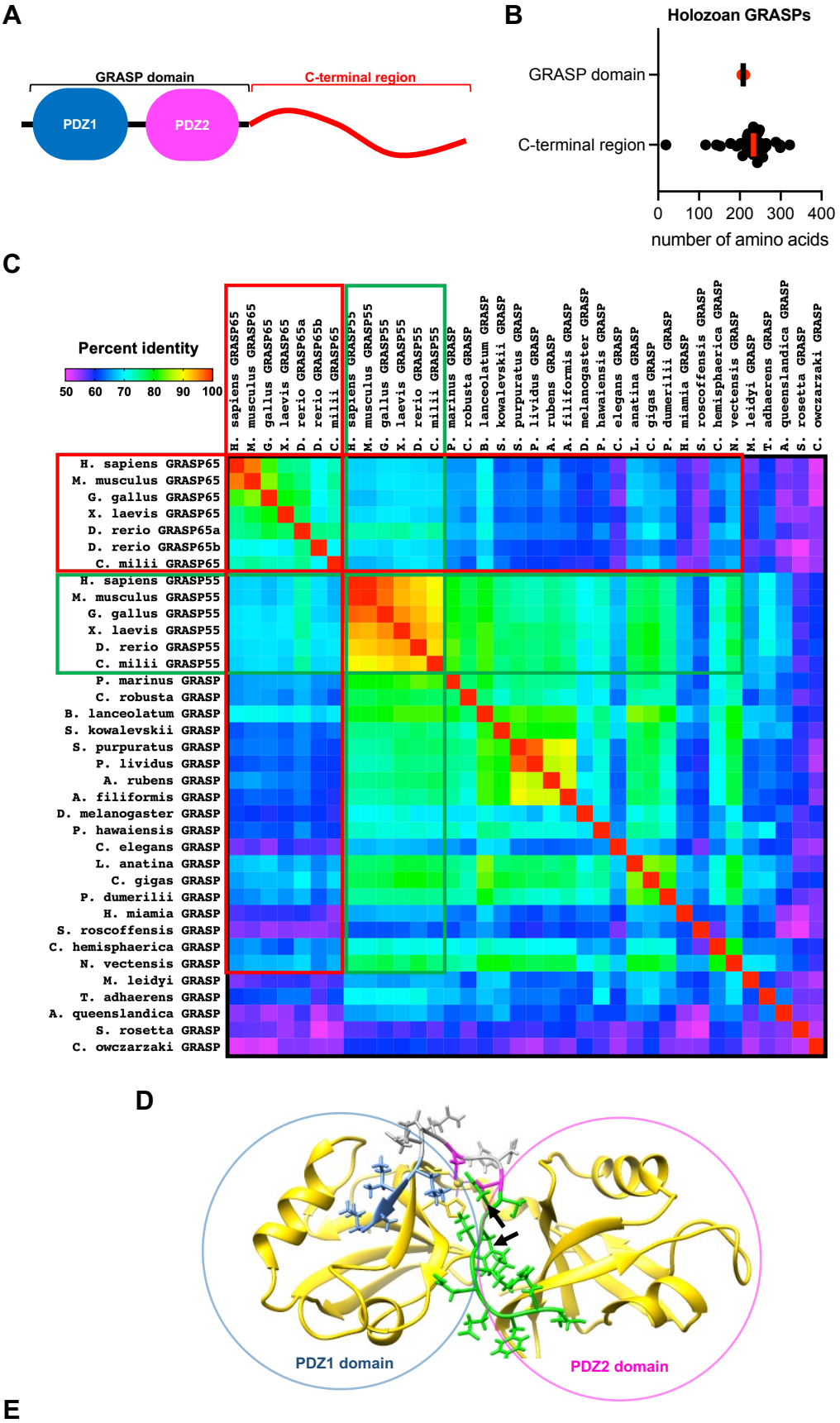
A
GRASP domain
C-terminal region
PDZ1
PDZ2
B
Holozoan GRASPs
GRASP domain
C-terminal region
0
100
200
300
400
number of amino acids
C
Percent identity
50
60
70
80
90
100
H. sapiens GRASP65
M. musculus GRASP65
G. gallus GRASP65
X. laevis GRASP65
D. rerio GRASP65a
D. rerio GRASP65b
C. milii GRASP65
H. sapiens GRASP55
M. musculus GRASP55
G. gallus GRASP55
X. laevis GRASP55
D. rerio GRASP55
C. milii GRASP55
P. marinus GRASP
C. robusta GRASP
B. lanceolatum GRASP
S. kowalevskii GRASP
S. purpuratus GRASP
P. lividus GRASP
A. rubens GRASP
A. filiformis GRASP
D. melanogaster GRASP
P. hawaiensis GRASP
C. elegans GRASP
L. anatina GRASP
C. gigas GRASP
P. dumerilii GRASP
H. miamia GRASP
S. roscoffensis GRASP
C. hemisphaerica GRASP
N. vectensis GRASP
M. leidyi GRASP
T. adhaerens GRASP
A. queenslandica GRASP
S. rosetta GRASP
C. owczarzaki GRASP
D
PDZ1 domain
PDZ2 domain
E
H. sapiens R----------YENIT----------FNCCNHCRG-EL-IAL
M. musculus R----------YENIT----------FNCCNHCQG-EL-IAL
G. gallus R----------YEDIT----------FNCCDHCQG-EL-IAL
X. laevis R----------YENIT----------FNCCNQCRG-EL-IAV
D. rerio R----------YENIT----------FNCCNQCNG-EL-IVL
C. milii R----------YENIT----------FNCCERCHG-EI-IVL
P. marinus R----------YEHIT----------FTCCSRCTG-DI-VVV
C. robusta Q----------HENIT----------LNCCVNCKG-EI-HVI
B. lanceolatum K----------YEEIT----------VNCCDKCKG-EI-KVV
S. kowalevskii N----------YENLT----------INCCPYCTG-DI-KVV
S. purpuratus C----------YENIT----------INCCDRCTG-DI-KVV
P. lividus R----------YENIT----------INCCDRCKG-DI-KVV
A. rubens T----------YENLT----------VNCCKYCKG-DI-KLV
A. filiformis K----------YENLT----------INCCNYCTG-DL-LVV
D. melanogaster P----------ASEVT----------PACDNQQLDKMQ
P. hawaiensis R----------HSSVK----------YI-KL
C. elegans K----------YTNLT----------IACCKNCMGRDI-QLL
L. anatina R----------FEQLT----------FCSCKHCSG-EI-QVV
C. gigas N----------FDNLT----------FNCCEKCKG-EL-TAV
P. dumerilii R----------YENIT----------FNCCSNCLG-EL-QVV
H. miamia N----------FDNLE----------FFSICKCCKNNTI-EVV
C. hemisphaerica T----------NYNVT----------FNCCEKCKG-PI-YIV
N. vectensis N----------SFRVT----------YDCCDRCTG-PV-HVV
M. leidyi L----------QQNVNGKMRE----------LFVACKTQQN-LI
T. adhaerens D----NSSTPSK---QTLYGS--------NKNVT---RSYSGC---KKTMFVGGCKSCAEKEI-LHL
A. queenslandica DDRH-DGNNDI----------ANNNS----------YYFCNKCNGRAI-MII
C. owczarzaki PSNHFDSATPISLGVSNLINSAEEDYSPALERVTTLMRERTSTMPSNSSQLLDCCKACRG-PI-IHL

Figure S4

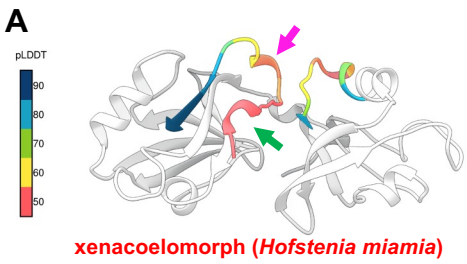
A
pLDDT
90
80
70
60
50
xenacoelomorph (*Hofstenia miamia*)

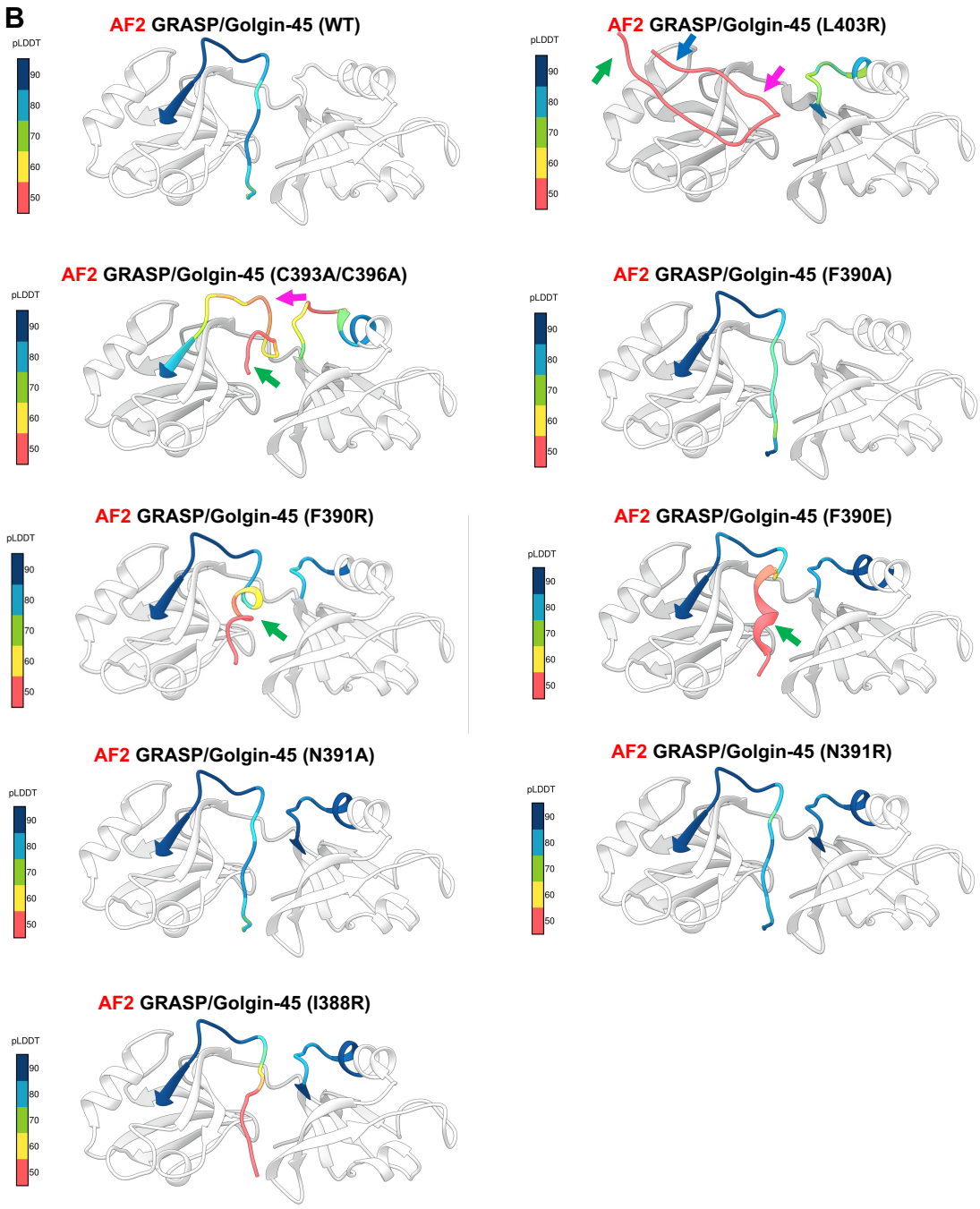
B
AF2 GRASP/Golgin-45 (WT)
AF2 GRASP/Golgin-45 (L403R)
AF2 GRASP/Golgin-45 (C393A/C396A)
AF2 GRASP/Golgin-45 (F390A)
AF2 GRASP/Golgin-45 (F390R)
AF2 GRASP/Golgin-45 (F390E)
AF2 GRASP/Golgin-45 (N391A)
AF2 GRASP/Golgin-45 (N391R)
AF2 GRASP/Golgin-45 (I388R)
pLDDT
90
80
70
60
50